

POLITECNICO DI TORINO

DEPARTMENT OF MECHANICAL AND AEROSPACE  
ENGINEERING

MASTER THESIS

in *Biomedical Engineering*

Analysis of breathing effect on  
vena cava



Politecnico  
di Torino



**Supervisors**

Prof. Luca Mesin

Doc. Piero Policastro

**Candidate**

Donatella Serra

Academic year 2022/2023



*To my family, friends and my sweet half.*

*I would not be here without you.*

# Contents

<b>1</b>	<b>Introduction</b>	<b>7</b>
<b>2</b>	<b>Background notions</b>	<b>9</b>
2.1	Cardiovascular system . . . . .	9
2.1.1	Cardiac cycle . . . . .	9
2.1.2	Arterial system . . . . .	11
2.1.3	Venous system . . . . .	12
2.1.3.1	Vena cava . . . . .	13
2.2	Ultrasound . . . . .	14
2.2.1	Physics principle of ultrasounds . . . . .	14
2.2.2	Structure of ultrasound device . . . . .	19
2.2.3	Probes . . . . .	20
2.2.4	Artifacts in ultrasound . . . . .	21
2.3	Respiratory system . . . . .	23
2.3.1	Pulmonary ventilation . . . . .	24
2.4	Spirometry . . . . .	27
<b>3</b>	<b>Software and instruments</b>	<b>29</b>
3.1	VIPER . . . . .	29
3.1.1	Scope and functioning . . . . .	29
3.2	Ecograph . . . . .	30
3.2.1	Probe . . . . .	31
3.3	Spirometer . . . . .	31
3.3.1	Pressure sensor and acquisition board . . . . .	34
3.3.2	CFD analysis and dimentioning . . . . .	38

<i>CONTENTS</i>	5
3.3.3 Limitation and approximation . . . . .	45
3.3.4 Spirometer results verification . . . . .	45
<b>4 Methodology and protocol</b>	<b>49</b>
4.1 Protocol . . . . .	51
<b>5 Results analysis</b>	<b>53</b>
5.1 First type of acquisition . . . . .	53
5.2 Second type of acquisition . . . . .	58
5.3 Third type of acquisition . . . . .	62
5.4 Fourth type of acquisition . . . . .	65
5.5 Fifth type of acquisition . . . . .	69
<b>6 Discussion and future developments</b>	<b>73</b>
<b>7 Conclusion</b>	<b>77</b>



# 1. Introduction

This master thesis aims to correlate breathing and vena cava's variations. It will be done thanks to a built spirometer and an ultrasound probe used at the same time.

It is known that the diameter of IVC (inferior vena cava) varies with cardiac cycle and breathing. Indeed, its diameter tends to increase during exhalation and decrease during inspiration. This happens because of a variation of pressure and the intervention of muscles. Whereas, regarding the cardiac cycle, the diameter is smaller right before atrial systole and it is bigger during atrial contraction.

In the clinical field, the evaluation of changes in vena cava diameters is widely used, which plays a key role in analysing and diagnosing clinical diseases. For instance, it is possible to evaluate CVP (central venous pressure) via vena cava variation [1]. Moreover, its variation of diameter is widely used to analyse the fluid responsiveness of patients with acute circulatory failure. Lastly, it can be used to estimate RAP (right atrial pressure) which, normally, requires an invasive procedure, that can be used in a few cases, by inserting a pressure sensor inside the right atrium: right heart catheterization (RHC).

Today the Caval index, the ratio between the difference of maximum diameter and minimum diameter and the maximum diameter, is used in echocardiography as a diagnostic indication to monitor cardiac function and the amount of blood returning to the heart during breathing. To calculate this, very often a technique known as sniffing is used, in which the patient is asked to perform a very strong nose inhalation.

As this technique is very dependent on the collaboration of the patient, this thesis sought to find a method to normalise an effort and make it possible for

each patient.

One of the biggest problems in estimating the diameter of IVC is its movement due to respiration. The greatest movement occurs in the craniocaudal direction. This causes different locations of ICV at different times, resulting in a decrease in its diameter. [2]

In order to try to reduce this problem as much as possible, it has been developed A semi-automated software, by VIPER (Vein Imaging Processing for Edge Rendering), to help clinics to follow, during imaging, the ICV in both longitudinal and transverse planes.

The next chapters give an overview of the cardiovascular and respiratory systems, as well as an explanation of how ultrasonography and spirometry work. This is followed by a full discussion of the spirometer's development and production processes. Finally, utilising a patient, the results will be shown, and potential future developments will be investigated.

## 2. Background notions

### 2.1. Cardiovascular system

The cardiovascular system is a very complex apparatus responsible for transporting blood into the body. It can be divided in two different ways:

- Arterial system
- Venous system

The first one takes blood from the heart to the body, whereas, for the venous system, it is the opposite. It is important to define the core of this system before getting to know how each one works.

#### 2.1.1. Cardiac cycle

The cardiac cycle represents the events that occur in each heartbeat. It can be divided into two main phases:

- Systole: It represents the ventricular contraction, in which the pressure increases
- Diastole: It represents ventricular relaxation, In this phase, the pressure falls

It should be noticed that blood flows from high pressure to lower. This is similar to the valves, which open because of a gradient of pressure. The atrioventricular valves separate atria from ventricles, they prevent the backflow of blood; the right one is the tricuspid valve, while the left one is the bicuspid

valve (mitral valve).

The semilunar valves are divided into the one that separates the heart from the aorta (aortic valve) and the other that separates the heart from the pulmonary artery.

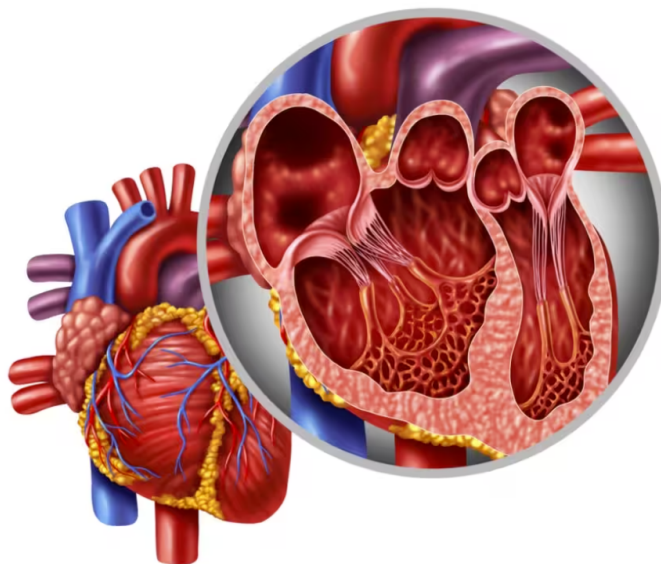


Figure 2.1: Heart valves

The first phase is the depolarization of the atria, it corresponds with the P of an ECG. This is the beginning of a diastole. The pressure in the atrium grows, the moment that the pressure is higher than the one in the ventricles the AV valves open. In this moment the blood starts to flow from the atrium to the ventricle. At the moment the contraction stops the pressure in the atrium starts to fall, so the pressure gradient is inverted and the valves close.

The second phase is characterised by the beginning of the systole. Here takes place ventricular depolarization, which corresponds to the complex of QRS in the ECG. Lunar valves stay closed until the pressure in the ventricles is lower than the one present in the aorta and pulmonary arteries. So, there is an isovolumetric contraction of the ventricles.

In the third phase, the pressure in the ventricles is high enough to let the lunar valves open.

The fourth phase is characterised by a pressure drop in ventricles. This causes the closure of the lunar valves. When the pressure is low enough to be lower than the one present in the atrium the AV valves open, it is the end of the systole and the beginning of diastole. Another cycle starts. [3]

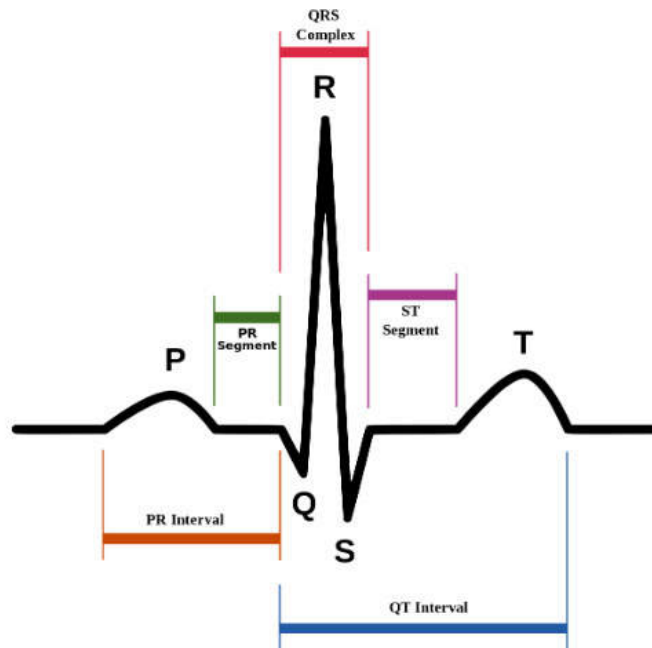


Figure 2.2: ECG

### 2.1.2. Arterial system

Considering the path that the blood has to accomplish, often, the vascular system is referred to as the circulatory system, due to its conformity. It is made up of two parts:

- Polmonary cycle: connects columnar vases to heart
- Sistic cycle: connects heart to all body's organs

There is a parallel organization all the organs are reached at the same time. The arterial system is responsible for taking the blood from the heart to all organs. It is characterised by several arteries that can be divided based on their dimension and diameter. There are the large arteries (elastic arteries),

such as the aorta, the medium arteries (muscular arteries), the small arteries and the capillaries.

Arteries are characterised by several layers:

- **Intima:** It is the interface with blood, it is one layer of endothelial cells. Under it, there is the basal lamina, made of connective tissue. It acts as a support layer
- **Media:** It is made up of muscular and elastic fibres. It is responsible for the mechanical response of the vase, it allows contraction and expansion. Under it, there is the external elastic lamina.
- **Aventitia:** there are fibroblasts, vasa vasorum, nerves and elastic fibres. It enables blood to flow all over the body. Moreover, it anchors arteries to nearby tissues.

Arteries carry very energetic blood, they have to earn as much energy as possible to give it back during systole. They need to be very compliant, for this reason, they are mainly composed of elastin.

Considering that the pressure in the arteries is quite high, the circumferential resistance needs to be elevated. This is why they have a spherical shape, which is not seen in veins, which are almost elliptical-shaped vessels due to the low pressure inside them.

### 2.1.3. Venous system

Regarding the venous system, the blood that flows in the veins has lower energy, for this reason composition of veins has to differ from the one of arteries. They are mostly composed of muscular fibre, because of the lack of fluid energy, so they have to push back the blood toward the heart. In addition, they have an inner valve not allow backflow, which is absent in the arteries.

The pressure in veins is much lower than the one present in arteries, for this

reason, they need to be pre-tensioned, to avoid complete closure of veins during the bending of the body part, this phenomenon is known as *kinking*. In contrast to arteries, they are characterised by a bigger longitudinal resistance.

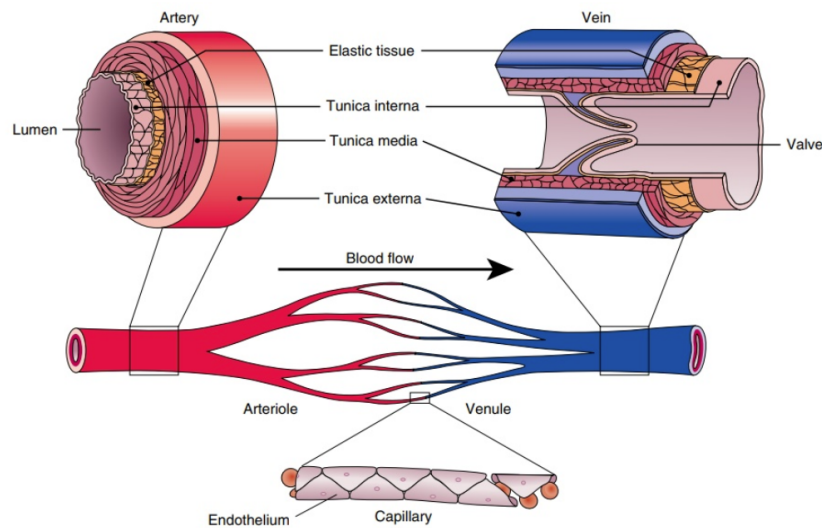


Figure 2.3: Differences between arteries and veins

### 2.1.3.1 Vena cava

Vena cava is divided into Superior Vena Cava (SVC) and Inferior Vena Cava (IVC). The first one is generated from the union of the right and left Cephalic veins, in the right part of the body. It takes the blood from the superior part of the body, such as the head and arms except for the lungs, to the right atrium. The IVC must collect venous blood from the inferior parts of the body, for instance, the legs or abdomen and take it to the right atrium. The SVC starts, roughly, where the first rib meets the manubrium. It is a few centimetres long. It does not have any valve inside.

The IVC forms by the union of the left and right common iliac veins to finish in the right atrium. It is the biggest vein in the human body, with a diameter of  $\sim 3.5\text{cm}$ . [4]

The size of the IVC and the amount of the change in that vessel's size are both

impacted by any manoeuvre or pathological state that modifies the pressure and volume of blood in the abdominal compartment. Because it enables the examination of several essential situations, the study of the size and pulsatility of the IVC is of particular relevance in the clinical environment. It enables the evaluation of cirrhosis and pulmonary fibrosis cases, the extraction of data on right heart function, the patient's right atrial pressure (RAP) and the patient's blood volume status. [5]

## 2.2. Ultrasound

This imaging technique uses the transfer of mechanical energy to the underlying tissues, for this reason, it is not ionising, it can be used for a quite long time and even on fragile patients, such as pregnant women. It is considered to be user-friendly. Moreover, it has a good time resolution, so it can be used to evaluate movement. It is based on reflection and diffusion.

Regarding ultrasound, there are 3 modes: A-mode, B-mode and M-mode. The first one is no longer used, but the other two are both valid solutions. The B-mode, B stands for brightness, it is quite useful for seeing movement in real-time. It is grayscale; also the M-mode is used to estimate movements, but it lets you draw a line and see, for each frame, the A-scan as a function of time.

### 2.2.1. Physics principle of ultrasounds

Ultrasound is sounds with frequencies that go beyond the threshold of audibility by the human ear, which means  $f \geq 20kHz$ . These are mechanical elastic waves, which have a compression phase when they assume a positive value, and a rarefaction phase when they are negative. Propagation speed depends on the elasticity of the mean in which they propagate. Despite these positive sides, it also has negative ones: the quality of ultrasound depends on who is

doing it, so a lot is up to the operator; it is hard to obtain good imaging if the patient is overweight; lastly, it cannot analyse structure under bones or gases, which act as shielding objects.

A mathematical law that defines the speed of propagation in the medium ( $v$ ) is:

$$v = \lambda \cdot f \quad (2.1)$$

where  $\lambda$  is wavelength and  $f$  defines the frequency of the wave.

It is also necessary to define the acoustic impedance ( $Z$ ):

$$Z = \rho \cdot v \quad (2.2)$$

where  $\rho$  is the density. US (ultrasounds) find resistance when they try to propagate in the medium. In general, the US cannot distinguish tissues by their density.

Each body, or in our case organs, has a different acoustic impedance

Material	Density	Propagation speed	Acoustic impedance
Air	1.2 [ $kg/m^3$ ]	330 [ $m/s$ ]	0.0004 [ $kg/m^2/s \cdot 10^6$ ]
Water	1000 [ $kg/m^3$ ]	1480 [ $m/s$ ]	1.48 [ $kg/m^2/s \cdot 10^6$ ]
Soft tissue	1060 [ $kg/m^3$ ]	1540 [ $m/s$ ]	1.63 [ $kg/m^2/s \cdot 10^6$ ]
Liver	1060 [ $kg/m^3$ ]	1550 [ $m/s$ ]	1.64 [ $kg/m^2/s \cdot 10^6$ ]
Muscle	1080 [ $kg/m^3$ ]	1580 [ $m/s$ ]	1.70 [ $kg/m^2/s \cdot 10^6$ ]
Fat	952 [ $kg/m^3$ ]	1459 [ $m/s$ ]	1.38 [ $kg/m^2/s \cdot 10^6$ ]
Brain	994 [ $kg/m^3$ ]	1560 [ $m/s$ ]	1.55 [ $kg/m^2/s \cdot 10^6$ ]
Kidney	1038 [ $kg/m^3$ ]	1560 [ $m/s$ ]	1.62 [ $kg/m^2/s \cdot 10^6$ ]
Lung	400 [ $kg/m^3$ ]	650 [ $m/s$ ]	0.26 [ $kg/m^2/s \cdot 10^6$ ]
Bone	1912 [ $kg/m^3$ ]	4080 [ $m/s$ ]	7.80 [ $kg/m^2/s \cdot 10^6$ ]

Table 2.1: Acoustical impedance and speed propagation

Usually for biological tissue it is considered the speed of propagation in the

medium is equal to  $1540m/s$ .

For mechanical waves, it is important to define certain parameters that characterise them:

- Amplitude: it is the maximum variation of the wave
- Wavelength: it is the distance between two adjacent ridges. It is the idea of the minimum spatial resolution that it is possible to distinguish
- Frequency: it is the inverse of period, and it is defined in Hz. It represents the number of times that the wave repeats itself each second
- Intensity: it is the rate of energy flow per unit of area

For wave generation, it is fundamental to understand the piezoelectric effect.

There are two different effects:

- Direct piezoelectric effect: a variation of length is followed by a variation of potential. It can be used as a receiver of US
- Indirect piezoelectric effect: a variation of potential is followed by a variation of length. It is the generator of US

In the US, usually, the piezoelectric material is PZT (lead zirconate titanate), in which has been calculated a speed of propagation of  $\sim 4000m/s$ . To obtain the depth reached by ultrasound it is possible to use:

$$h = \frac{\lambda}{2} = \frac{v}{2 \cdot f} \quad (2.3)$$

Acoustic waves are easily focused: simply place an acoustic lens in front of the crystal, and focus the acoustic field at a precise point, depending on the curvature of the wave, a longer or shorter beam is obtained.

As it has been said before, what is seen on the screen is the reflection of the mechanic wave, for this reason, it is necessary to introduce Snell Law.

$$\frac{\sin\theta_i}{\sin\theta_t} = \frac{n_1}{n_2} \quad (2.4)$$

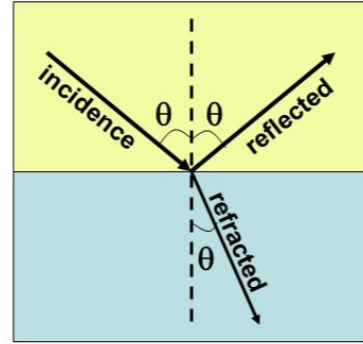


Figure 2.4: Snell law

When a wave meets a separating surface its velocity of propagation varies. The incident beam impacts on a mean, a part of it passes through the medium with an angle of  $\theta_t$ , while the remaining part gets reflected with an angle of  $\theta_r$ . Snell affirms that the angle of incidence and reflection are the same. On the other hand, the angle of incidence and the angle of refraction are linked by a sine ratio. In ultrasound reflected rays are the ones of interest.

Considering what has been said till now, it must be introduced other two variables: reflection coefficient (R) and transmission coefficient (T).

$$R = \frac{\operatorname{tg}^2(\theta_i - \theta_t)}{\operatorname{tg}^2(\theta_i + \theta_t)} \quad T = 1 - R \quad (2.5)$$

T is a parameter that describes how much of a wave is reflected by an impedance discontinuity in the transmission medium. R represents how much a wave is reflected when it meets an impedance discontinuity in the medium. So, if something does not get reflected it passes through the body, for this reason, the sum of the reflection coefficient and transmission coefficient is equal to one.

For ultrasound, there are intrinsic limitations:

- If the acoustic impedance of the two materials constituting the discontinuity is similar then, R takes on very low values. This problem is known as detectability.
- If one of the two means is the air  $R \sim 1$ , for this reason, it is required to use gel between the body, which has to be analysed, and the probe, in order to avoid this huge difference in reflection coefficients.

The frequency used in ultrasounds is much bigger than the audible frequency (20 kHz), usually the frequency used is in the order of MHz. The frequency chosen determines the depth of acquisition, the higher the frequency, the more superficial the analysis will be, but it is more accurate. If it is necessary to acquire something deeper it is necessary to a smaller frequency.

When a material is hit by a mechanical wave it absorbs a part of it, so it undergoes an attenuation (A).

$$A(Z) = A_0 \cdot e^{\alpha \cdot z} \quad (2.6)$$

Where  $\alpha$  represents the absorption coefficient and  $z$  is the depth. The absorption is the reason why the US cannot go through bones, they absorb all the beam. If the frequency increases even the absorption increases.

It is known, from physics, that two points at a distance less than the wavelength cannot be revealed as distinct, but, referring to the US, there is not only a wave but a package of waves, in this way the resolution of a single sinusoid is smaller than the wavelength.

In any case, if the wavelength of the impulse is bigger than the distance between two objects, the echo returning to the source will be only one, so it is impossible to identify two different objects. But if it is bigger there will be two returning echoes, so the objects will be considered as separated. To sum up, real resolution coincides with the duration of the package.

It can be distinguished three different types of resolution:

- Axial resolution: capability to distinguish two objects that are on the path of ultrasounds, namely that move away from the probe
- Lateral resolution: the capability to distinguish objects that are at the same distance from the probe, but placed sideways
- Slice thickness resolution: capability to distinguish two objects that are at the same distance from the probe, but placed in two different planes

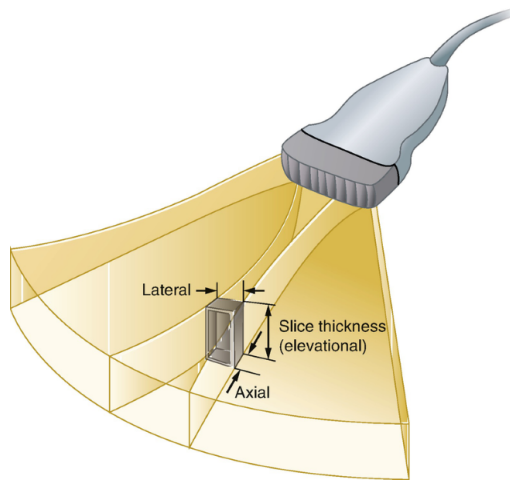


Figure 2.5: Ultrasound's resolution

### 2.2.2. Structure of ultrasound device

Ultrasound machine is composed of three main parts:

1. Probe: It is the part that interacts with the patient. There are various types of them, each one specific for each type of ecography.
2. Ultrasound generator: This part generates the US through a piezoelectric material at a high frequency of the order of MHz.
3. Electronic part: it is needed to receive and analyse return echoes to elaborate the image

This imaging technique uses the principle of reflection. Indeed, when the probe emits a wave it enters the body and travels inside of it, when it meets objects with a coefficient of reflection different from the one of the body, it comes back as an echo. It is possible to evaluate the distance or depth of the object found by evaluating the flight time of the wave.

$$d = \frac{1}{2} \cdot c \cdot \delta t \quad (2.7)$$

To obtain an image there are several steps:

- The cristal emits impulses
- Transducers receives the echos of return
- It is calculated flight time and, as a consequence, the depth
- The amplitude of the signal is proportional to the difference in acoustic impedance
- The echo is amplified by a factor proportional to the delay. It is possible to do so thanks to the TGC, time gain compensation. TGC balances the amplitude of echoes. It is a logarithmic amplification which takes in flight time. This guarantees that the amplitude of the echo is always the same.

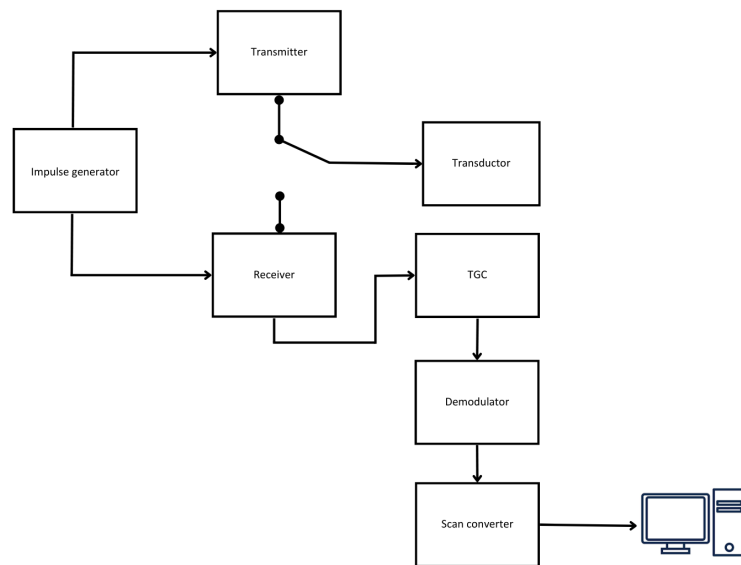


Figure 2.6: Flowchart of ultrasound

### 2.2.3. Probes

There are many types of probes, but the most commonly used are: linear, curvilinear and phased. The first one is mostly used to analyse superficial organs, for instance, superficial vascular or pедиатry.

It has huge frequencies, [5-10MHz], so it has a good resolution to the detriment of depth. The curvilinear probe has lower frequencies [2-5MHz], so it is used for deep tissue such as abdominal vasculature.

Phased arrays are less widespread than the other two; frequencies are 1-5MHz and it is used in transcranial and transthoracic vascular. In this thesis, it will be used the curvilinear one.[6]

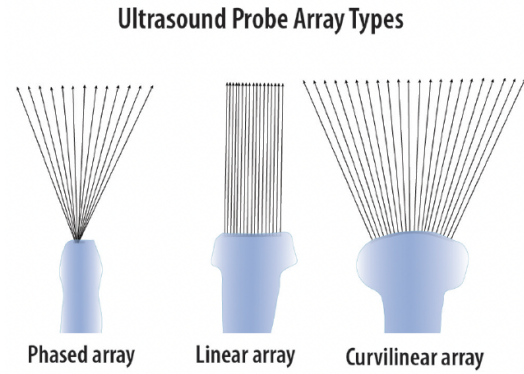


Figure 2.7: Ultrasound's probes

#### 2.2.4. Artifacts in ultrasound

Ultrasounds are affected by several artefacts, which can be caused by the operator or by the device. For the first type, they can be caused by a lack of formation of the operator, or because of an incorrect setting of parameters. It is even important to prepare correctly the patient and to use the correct scanning technique.

Sometimes, artefacts can help in diagnosis by contributing to the characterisation of the anatomical structure, but in other cases, they can completely alter the structure leading to incorrect diagnoses.

Here is a list of some artefacts:

- Reverberation: It occurs when the ultrasonic beam hits a highly reflective surface. The reflected ultrasound strikes the transducer and is then sent back into the tissue. This path is repeated several times, leading to multiple reflections between the object and transducer, producing a series of echogenic bands with decreasing intensities spaced at regular intervals that are equal to the distance between the object and probe.
- Ring down: It is a discernible artefact, it happens when the US meets

small, discrete and very bright close-range echoes, for instance, they can be small gas bubbles, microcalcifications or cholesterol crystals. It is a kind of reverberation artefact that results from several reflections that take place between an object's front and back walls. These produce a series of echoes close to each other, that resembles a comet tail.

- **Shadowing:** With this type of artefact there is a shadow zone, which means without echoes, caused by very reflective objects, such as bones, or very attenuating ones, solid tissue or malignant masses.
- **Rear wall reinforcement:** A homogenous liquid collection does not create echoes, considering the fact that is highly anechogenic, therefore ultrasound waves travelling through it attenuate significantly. However, the beam experiences the usual reflection, refraction, and attenuation effects at the side of the liquid collection. Therefore, ultrasounds that travel beyond the liquid collection are more intense than those that do not travel through the liquid collection itself. Tissues that are posterior to the liquid collection will generate considerably more powerful echoes than the surrounding tissues, giving them the appearance of being more echogenic.
- **Lateral refraction shadow:** as it happens for objects immersed in water, even the ultrasounds also undergo the phenomenon of refraction, for this reason, the image may be distorted. This distortion may lead the operator to believe that he is in the presence of a discontinuity in the continuum
- **Side-lobe artefact:** it is produced by minor ultrasound beams that do not travel along the primary beam axis and produce ghost echoes in the image. When these beams interact with a highly reflective interface back to the probe, the returning echoes are misplaced in the image, even though they did not originate from the main ultrasound beam and generate the artefact in question. To reduce artefacts from side beams

it is generally sufficient to decrease the overall gain in order to suppress echoes at low energy

- Mirror artefacts: This occurs when large and curved reflecting surfaces, such as the diaphragm-lung contact, are present. In these circumstances, a portion of the ultrasound beam is reflected, and artefacts are produced when the echo returns to the probe. To solve this problem, it is useful to remember that the real part will be present in all the visualisation, while there won't be the artifacted one.

## 2.3. Respiratory system

The respiratory system gives oxygen to tissues and cells; it eliminates  $CO_2$  that forms in the organism. Chemicals and nervous stimulus control ventilation frequency. It consists of the upper airway and respiratory tract. The first one is made up by:

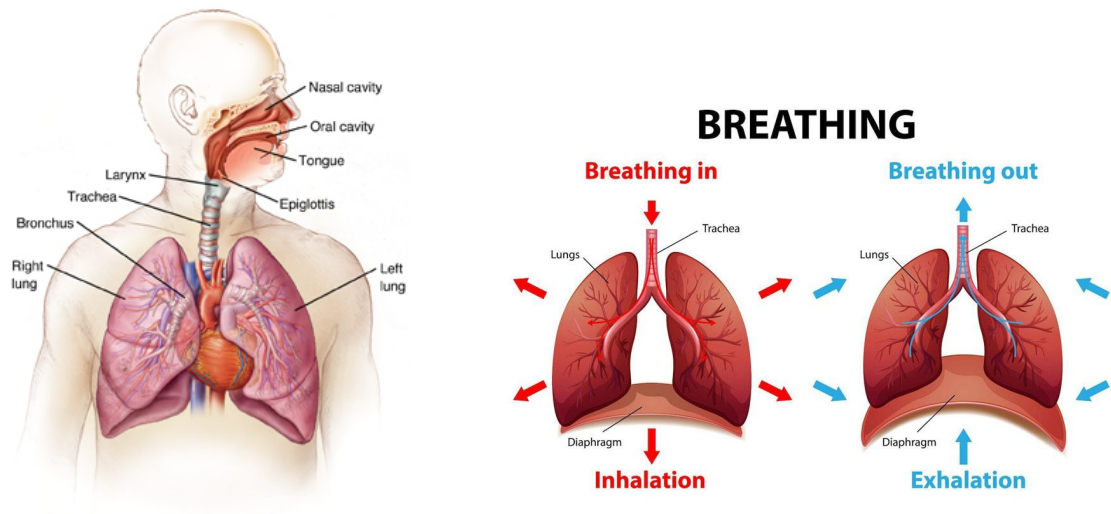
- Nasal cavity
- Pharynx
- Tongue

The second one:

- Larynx
- Trachea: semi-rigid duct with a diameter of  $\sim 2.5\text{cm}$  and a length of  $\sim 10\text{cm}$
- Bronchi
- Alveoli: gas exchange happens here.
- Lungs

- Diaphragm

During respiration, air comes into the body through the mouth or nasal cavity and it reaches the pharynx. Air moves toward the larynx and then it enters the trachea when the epiglottis is open. The trachea branches off into two primary bronchi, which in turn divide into 12 smaller bronchi. Air exchange happens at the level of the alveoli.



### 2.3.1. Pulmonary ventilation

The main part of this system is the lungs. They are situated in the rib cage, with the heart. They are limited by the diaphragm underneath. Each lung has no support structures, they are enclosed in a pleural sac which divides the lung from the rib cage; Inside it, there is the pleuric fluid which allows the sliding of the two sheets, and allows a strong adhesive strength among the lungs and thoracic wall.

In order to have a breathing act there must be a difference in pressure between the outside (atmospheric pressure) and alveoli.

Lungs are normally expanded compared to their equilibrium, while the cage rib is compressed. These two opposite strengths form the pleuric pressure, which is negative ( $-5 \text{ cmH}_2\text{O}$ ).

Breathing is ensured by a different pressure: if the alveolar pressure is lower than the atmospheric one, it is the natural condition, otherwise, it is the condition of artificial ventilation in which there is a positive pressure.

Breathing is characterised by two processes: inspiration and expiration. The first one is active, which means that to expand the lung it is necessary to contract inspiratory muscles (diaphragm, external intercostals, sternocleidomastoid, etc.). On the other hand, expiration is a passive process, unless it is a forced expiration, the muscles used are internal intercostals, abs, and accessories.

As we see in Figure 2.4 there is an inverse proportion between volume and pressure, but airflow follows the volume.

$$P = \frac{nRT}{V} \quad (2.8)$$

Breathing, that is the sum of inspiration, expiration and the pause, lasts  $\sim 4$  seconds; inspiration lasts  $\sim 1,2$  seconds, expiration is more or less 2 seconds and the pause lasts less than a second.

During inspiration, there is an increase in lung volume up to a peak.

Exactly the opposite of lung volume and airways happen for pleuric pressure and alveolar pressure, respectively.

Instead, regarding expiration it can be noticed a negative variation of volumes and airflow. For the second one, even in this case, it has a parabolic trend, but with the opposite sign. Even in this case pleuric pressure and alveolar pressure keep an opposite trend compared to volume variation and airflow.

In any case, it is important to notice that the first two are always positive, while

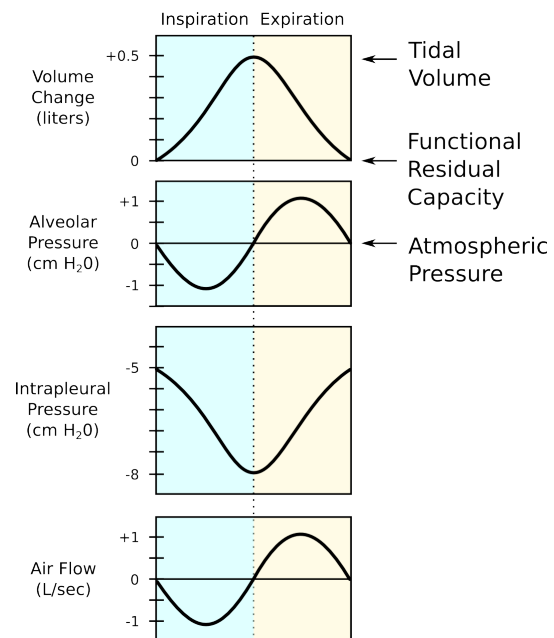


Figure 2.9: Relation between volume and pressure

The airflow increases until half of the

pleuric pressure is always negative. Alveolar pressure can be either positive or negative.

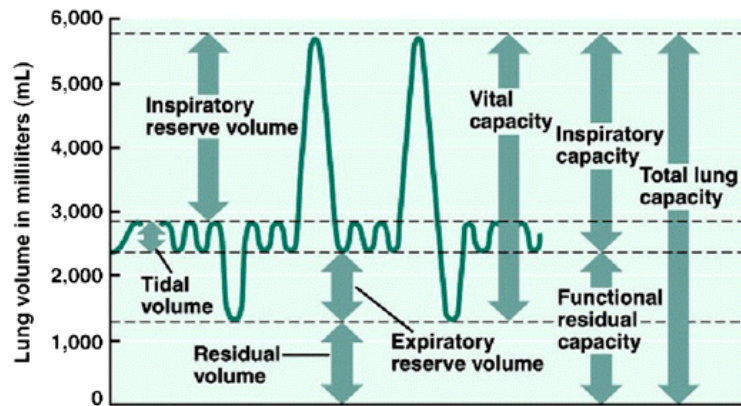


Figure 2.10: Lungs volume and capacities

To begin with, it is important to separate volumes and capacities. Talking about volumes, there are:

- Tidal volume: inspired and expired volume in a normal respiratory act ( $\sim 500$  ml)
- Inspiratory reserve volume: maximum volume that can be inspired from the end of a normal inspiration ( $\sim 3000$  ml)
- Expiratory reserve volume: maximum volume that can be exported from the end of a normal expiration ( $\sim 3000$  ml)
- Residual volume: maximum expirable volume from the end of normal expiration ( $\sim 1100$  ml)

Talking about capacities, there are:

- Vital capacity: maximum expired volume starting from a maximal inspiration
- Inspiratory capacity: maximum expired volume starting from an end-expiration volume

- Functional residual capacity: residual volume in lungs at the end of a normal expiration
- Total lung capacity: volume present in the lungs after maximal inhalation

## 2.4. Spirometry

Spirometry is a technique which allows the measurement of tidal volume, which means the lung volume during a normal breathing act. It is used to evaluate how much air you can breathe in and out. Usually, in normal measurements, the patient is sitting on a chair with the feet flat on the floor.

It is the most common test to evaluate pulmonary functionality. It can be performed both on healthy individuals and in subjects with pathologies.

It is asked to the patient to take a big breath and hold it for a few seconds. Later, after having put the spirometer in their mouth with a nose cap, the patient is asked to blast the air out of his lungs as hard and as fast as he can. It is necessary to repeat the experiment at least three times in order to obtain consistent data.

The invention of the spirometer goes back to John Hutchinson, a British surgeon, around the 1800s.

Spirometry is useful in diagnosing a huge variety of pulmonary diseases such as chest restriction. But, to obtain reliable results it is important to guarantee reproducibility, standardization, and a good quality of testing. With this technique, it is possible to measure both inhalation and exhalation but is far more used for the exhalation.

Among the four types of volumes only the residual volume cannot be measured. Even for capacities, the vital capacity and the functional residual capacity cannot be measured because they contain the residual volume.

Considering that the data can change among the population, it is important to apply the right equation according to age, gender, height, and ethnicity.

Spirometry uses a spirometer, a device often connected to a computer that plots flow and pressure trends in real time to obtain measurements.

The vital capacity is the principal outcome of spirometric measurements, which means the sum of maximal exhalation and maximal inspiration. The measure finishes when the patient is not capable of expelling air. [7]

## **3. Software and instruments**

In this master's thesis imaging techniques, such as spirometry and ultrasound, are used. These are used to scan patients while they are breathing inside the spirometer.

### **3.1. VIPER**

VIPER is a semi-automated software, implemented on Matlab, used to segment the inferior vena cava in post-processing. It makes it possible to segment in both longitudinal and transverse planes, but in this thesis, it has been used only in the longitudinal plane due to the high movements that made it impossible to follow the vein in the transversal plane.

#### **3.1.1. Scope and functioning**

The main scope of this software is to help clinics and doctors evaluate, in a more accurate way, the vein and its diameter. It is possible to use it in a semi-automated way in which it is necessary only to upload the video of the echography made on the subject; after that, it is asked to the operator to specify some things that vary depending on the plane of the vein. For the transversal plane, it is necessary to indicate the centre of the vein, while for the longitudinal it is asked to indicate: two points of reference that do not move much, for example, it can be advised to pick the hepatic veins; the first diameter of the vein with a point in the upper side and one on the lower side and, lastly, it is necessary to draw a line to indicate the end of the part of the

vein analyzed. The software gives results with 21 diameters calculated in each frame of the video.

As it has been said in the previous paragraph it could have been used the semi-automated software, but due to the huge amount of movements of the vein, it was impossible to use this type of segmentation because the vein moved away from the frame seen on the screen so the software could not follow it. To overcome this problem, a manual segmentation of the vein has been made. [8]

## 3.2. Ecograph

It has been used as a portable ecograph *MicrUs Ext-1H*, which has been developed by Teleded. It is compatible with several devices, such as computers, tablets or smartphones. Convex, micro convex, linear, and endo-cavitary probes are supported, and they may be utilised in several display modes, including B and M modes. Depending on the probe type and scanner model, the scanning depth can range from 2 to 31 cm. The system employs broad bandwidth multifrequency probes (2.0 to 15.0 MHz) to provide high-quality video and pictures in general, abdominal, obstetric, and gynaecological ultrasonography, among other applications.

The resulting image is greyscale, consisting of 256 tones. It also has a good frame rate and allows a zoom of the area of interest ranging from 60% to 600%. It allows data to be saved in various formats, such as .mp4 or .avi.

The MicrUs EXT-1H is provided with a few additional items:

- MicrUs EXT-1H Beamformer, the base unit
- USB Key with installation and set-up manual, User Manual, Software
- Transducers selected by the customer
- USB cable

### 3.2.1. Probe

For the probe, it was necessary to purchase one separately. It has been used as a Convex Probe, C5-2R60S-3, also manufactured by Telemed. It is composed of S3-type crystals that let it operate in a range of 2-5MHz. It is characterised by a curvature radius of 65mm and by a field of view of 60°. It is mainly used for ultrasound examinations performed in the abdomen, in obstetrics and gynaecology, and paediatrics.



Figure 3.1: Convex probe

## 3.3. Spirometer

In this master thesis, it has been developed a spirometer by using two differential pressure sensors and a 3D-printed Venturi tube.

The tube is characterised by three pins used to measure the differential pressure. They are located at 45mm after the inlet, 45mm before the outlet and at the middle of the bottleneck, to be more precise at 9cm after the inlet. The configuration of the Venturi Tube has been chosen due to its simplicity. Indeed, Venturi's effect says that a fluid that flows into a tube keeps constant the mass, which means that the product of the section and speed is constant. This conservation is valid only in an ideal situation when there are no dissipative effects, such as turbulence, so the tube needs to be quite long.

Initially, reference was made to the ISO-FDSI-5167-4 [9] standard which explains how a venturi can best be designed. It became apparent, however, that to have the size of the striction of the venturi tube used, a length not accessible

for spirometry was required. For this reason, it was decided to try to design a spirometer as similar as possible to the one described in the standard, albeit allowing for some approximations.

Nevertheless, the results of the spirometer built in this way are promising, so it has been possible to accept these approximations.

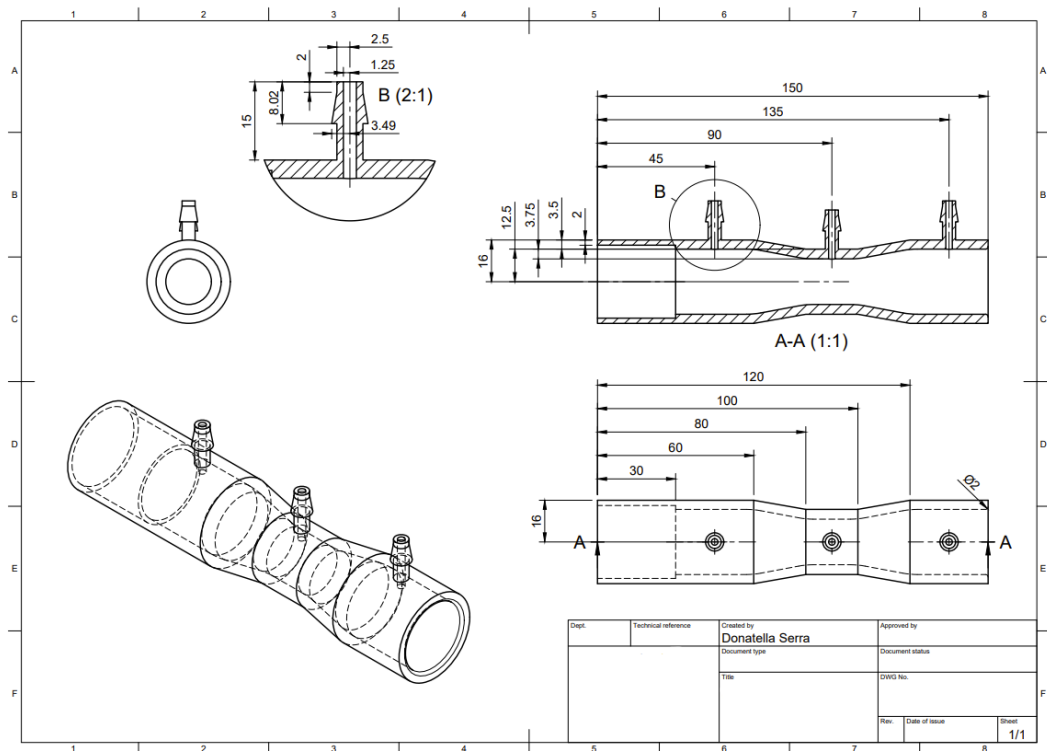


Figure 3.2: Spirometer dimentioning

The dimensions chosen are 15 cm length in which is inserted the sterile mouth-piece, of 10 cm, for 3 cm; the pins are equally spaced every 4.5 cm since the beginning of the tube, and internal fittings are characterised by a radius of 3 cm. The diameter of the entrance and the exit of the tube is 2.5 cm, while the one of the bottleneck is 1,75 cm.

Following several observations regarding the variation of the vein's diameter it has been thought to increase the muscular activation to increase the variation. Indeed, it has been built as a water tap, made like a venturi tube but with

a bottleneck smaller, to impose a bigger effort for the subject. Moreover an increase in the length of the spirometer, this water tap is put before the venturi tube with the pin for the measure, helps the sensors to be more precise by reducing turbulence.

It is made of the same material as the primary venturi tube and has the same diameter for the section of the entrance and the exit, while, the diameter of the bottleneck is quite smaller, indeed it measures 1 cm.

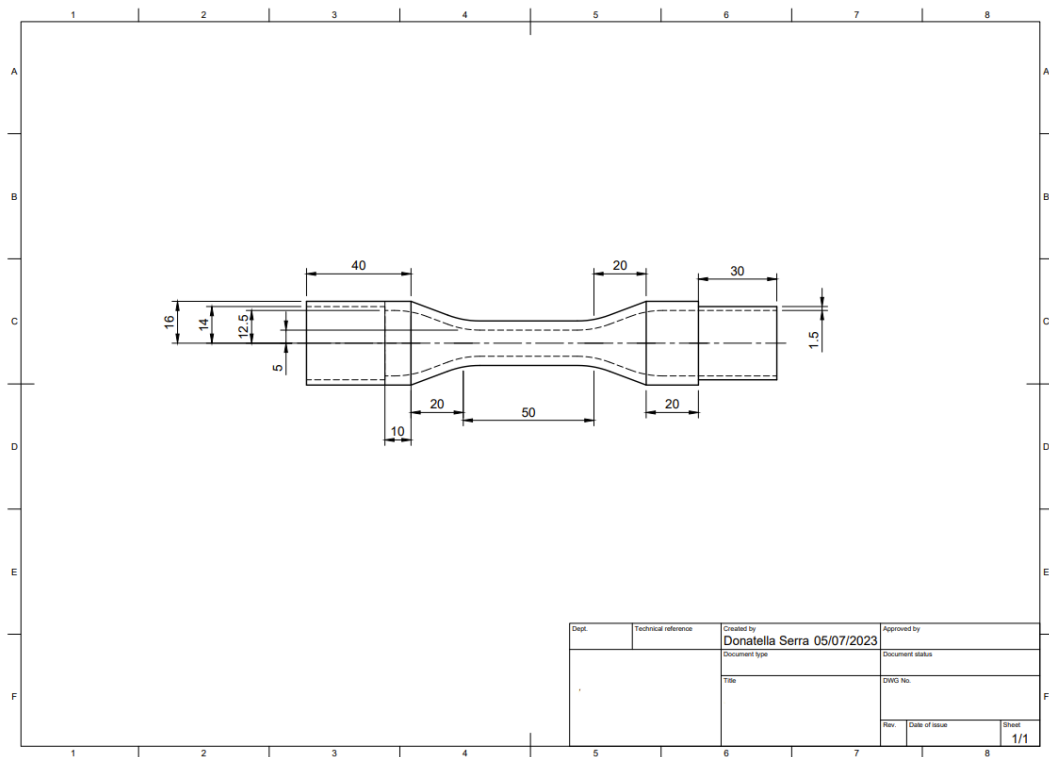


Figure 3.3: Tap dimentioning

To reduce the dimension of the eddies generated by the expiration and inspiration, it has been thought to use a net with little holes, in this way, the perturbation felt by the two sensors decreases strongly. Eddies are vortices formed as a result flow of the air being forced out of the patient's mouth, they vary a lot in size. In this way, the output in volt tends to oscillate much less. As proof one of the first measurements taken in the two cases is shown: one with the net and one without the net. It shows this problem very clearly.

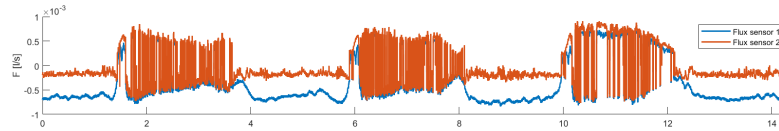


Figure 3.4: Flux without net

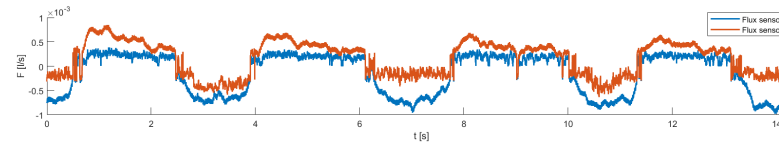


Figure 3.5: Flux with net

### 3.3.1. Pressure sensor and acquisition board

Two Sensirion SDP816 differential pressure sensors were employed in the construction of the spirometer, and a 3D-printed venturi tube was used for the sensor body.

It is designed to detect the pressure difference between two points. It is a solid-state sensor based on Sensirion’s CMOSens technology, which integrates a high-precision analogue-to-digital converter with a differential pressure sensor on a single chip. The SDP816 125Pa sensor’s working theory is based on how the applied differential pressure alters electrical resistance. A flexible layer serves as the sensor’s membrane, and it deforms in reaction to differential pressure. A sensing element’s resistance is altered by the deformation, and this resistance is changed into an electrical signal that is proportionate to the differential pressure. It has a 125 Pascal (Pa) measuring range with an accuracy of 1 Pa. The sensor’s 0.1 Pa resolution enables extremely accurate readings. It responds quickly, on the order of milliseconds, allowing instantaneous acquisition of pressure data. The sensor is calibrated to work in a temperature range of  $-20^{\circ}\text{C}$  to  $80^{\circ}\text{C}$  and it needs a small power source with an operating voltage between 2.2 V and 3.6 V.

To obtain the measurement in real-time on Matlab, it was necessary to use

a National Instruments USB 6001 acquisition board. It is widely used to acquire and elaborate signals. It is equipped with high-resolution, low-noise analogue-to-digital converters with 14-bit, which enable the acquisition of analogue signals with precision. Additionally, the gadget has a USB connection that makes it easier to interface with the host computer and guarantees quick and dependable communication between the device and the data acquisition software.

It has an input range and a working voltage of  $\pm 10V$ . It has a resolution of 32-bit and a maximum input frequency of 5 MHz. eventually, it has an output voltage of  $\pm 5V$ .

The output of the sensor is in volt and thus has only positive values, one sensor is not enough to identify the breathing phases: inhalation and exhalation. Two sensors were therefore used. In fact, at the inversion of the flux, which means during the passage between inspiration to expiration and vice versa, the two sensors, located at the same distance from the middle of the striction, see different  $\Delta P$ .

Indeed, as it can be seen by Figure 3.6, the output of the two sensors is always positive, but they invert their relative position during the phases of breathing. The first sensor, which is the blue one in the figure, is connected to the pin of the inlet and the bottleneck of the tube, while the second sensor, the red line, is connected to the pin of the outlet and the one of the bottleneck. During inspiration, the second sensor sees a differential pressure bigger than the first one, since the pressure at the part of the tube placed at the mouth is smaller than the one outside. During expiration, exactly the opposite happens as there is a higher pressure at the mouthpiece and a lower pressure at the tube outlet. To consider the bidirectional flux, caused by inspiration and expiration, it has been necessary to use an Output Curve Selection Input with the configuration of square root given by the datasheet of the sensor. With this configuration, it is possible to guarantee a more stable zero point and higher sensibility to

low pressures.

$$DP = \text{sign}\left(\frac{A_{OUT}}{VDD} - 0.5\right) \cdot \left(\frac{A_{OUT}}{VDD \cdot 0.4} - 1.25\right)^2 \cdot 133 \quad (3.1)$$

In this equation the DP is the differential pressure, VDD is the supply, and  $A_{OUT}$  is the ratiometric analogue voltage output.

It is always seen as a negative differential pressure because there is a subtraction of pressure between the pin located at, respectively, the bottleneck and the inlet and outlet of the venturi tube, which always have a bigger pressure. Considering the Bernoulli equation and the mass conservation can be found the flow as in Equation 3.4, in which the 2 stands for the outlet of the tube. The sign functions are used for bi-directionality.

$$P + \frac{1}{2}\rho v^2 + \rho gh = \text{constant} \quad (3.2)$$

$$v_1 \cdot A_1 = v_2 \cdot A_2 \quad (3.3)$$

$$F = \text{sign}(\Delta P) \cdot v_2 \cdot A_2 = \text{sign}(\Delta P) \cdot A_2 \cdot \frac{2\Delta P}{\rho\left(1 - \left(\frac{A_2}{A_1}\right)^2\right)} \quad (3.4)$$

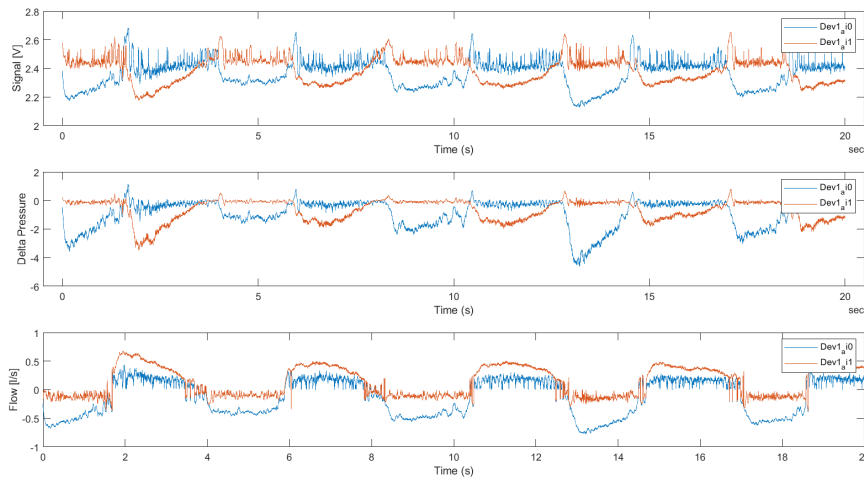


Figure 3.6: Output of sensor and conversion to flux

In Figure 3.7 it can be seen a pressure trend as velocity and area ratio change. Variable speeds between 1 and 8 were considered in step one to see the pressure imposed on the subject caused by the constriction.

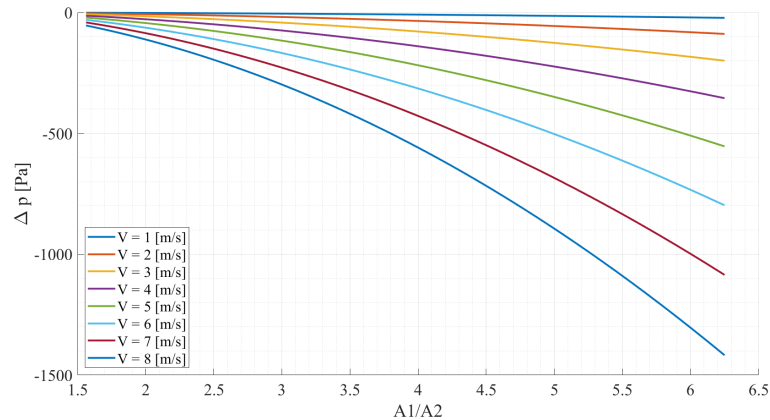


Figure 3.7: Relation between pressure and area ratio

The final setup of the spirometer with the two sensors and the acquisition board is like the one in Figure 3.8, in which the number 1 is the breadboard used to connect the pin of the sensors (number 2) to the acquisition board (number 3). The sum of number 4 (the mouthpiece that needs to be inserted in the tube), number 5 (principal venturi tube), number 6 (the tap) and number 7 (the net) is the complete set utilized as a spirometer.

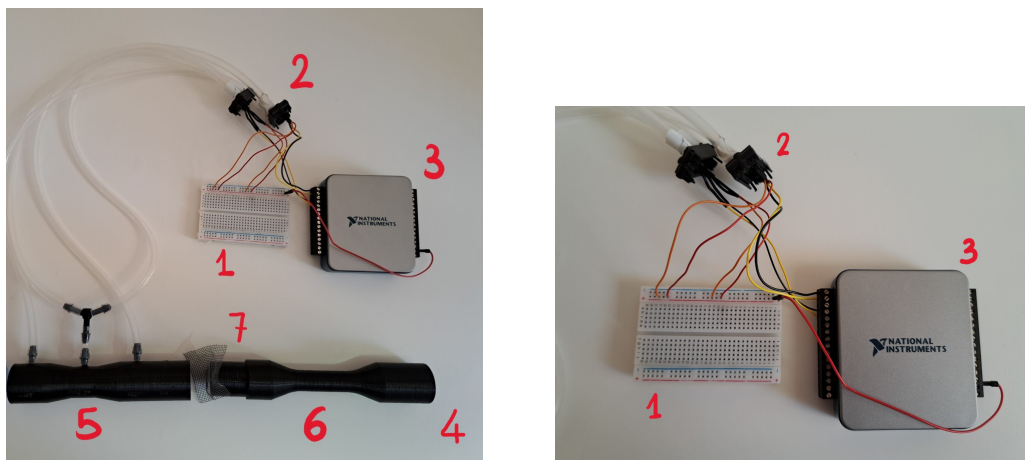


Figure 3.8: Spirometer

### 3.3.2. CFD analysis and dimentioning

Parallel to the analytical study conducted, considering the well-known approximations, an approximate CFD was carried out to assess the sizing of the designed pipe.

This analysis simulates an exhalation at a constant speed of 2 m/s in the steady state. This type of simulation is not indicative of a real, instantaneous situation, but a kind of time average of what is happening in the duct with a constant flow within it. Turbulence is modelled using a model  $K\varepsilon$ , the length of the vortices was set at 1.5 mm, which is equivalent to the mesh size of the net used to make the turbulence isotropic.

The CFD domain consists of half a venturi tube cut horizontally, given the symmetry of the tube, on which a symmetry constraint was imposed on the lower wall.

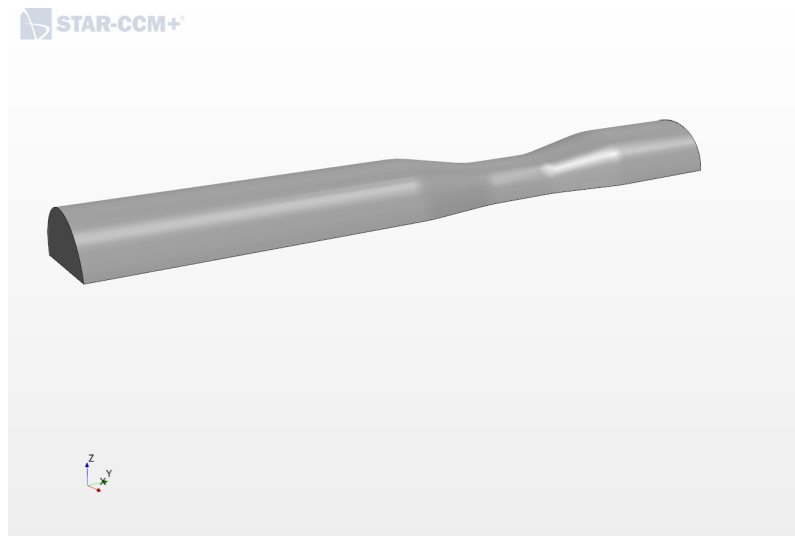


Figure 3.9: Domain of CFD

The domain was discretised using Star CCM+'s automated mesh command, with a hexagonal cell base size of 0.25mm and a prism layer of 1.5mm in height. This layer makes the mesh denser, which means elements smaller, in correspondence with the edge, slowly incrementing their dimension towards

the centre, where the mesh becomes less dense.

The boundary conditions applied are:

- Wall: A zero wall velocity is imposed
- Inlet: The inlet flow is placed at a constant velocity of 2 m/s along the spirometer axis
- Outlet: Pressure is set constant and equal to ambient pressure
- The spirometer base is considered symmetrical

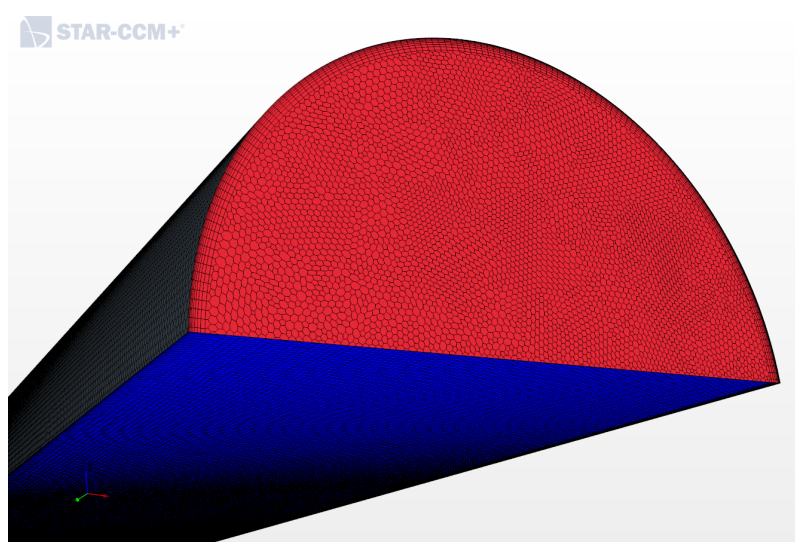


Figure 3.10: Mesh

The simulation was conducted by decoupling the energy equations, thus only considering momentum and continuity. It is noted that, after an initial rapid decrease of the residues, the simulation was allowed to continue by stopping it at 600 iterations, where although further decreases can be expected, it was decided to stop it to contain the calculation time.

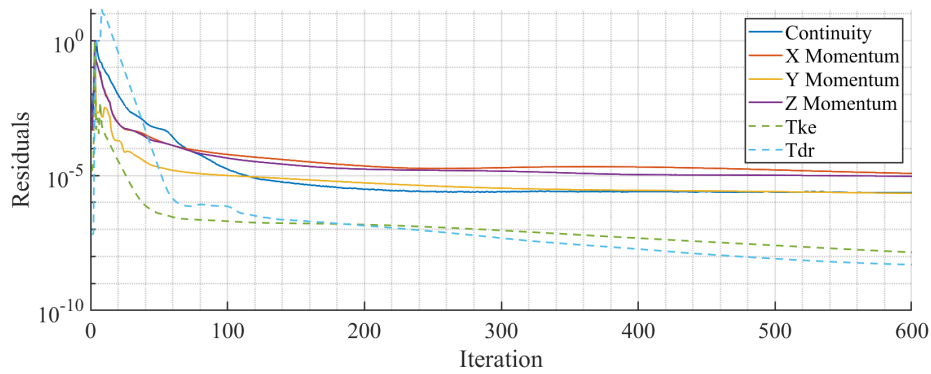


Figure 3.11: CFD residuals

The images shown below represent sections in one or more planes of the duct. Looking at the pressure field seen in Figure 3.12, it can be seen a clear decrease in pressure at the bottleneck with a subsequent increase. In general, there is a higher pressure at the inlet. This happens because to exhale, the air must pass from a place with a higher pressure to one with a lower pressure due to a pressure gradient that needs to be compensated.

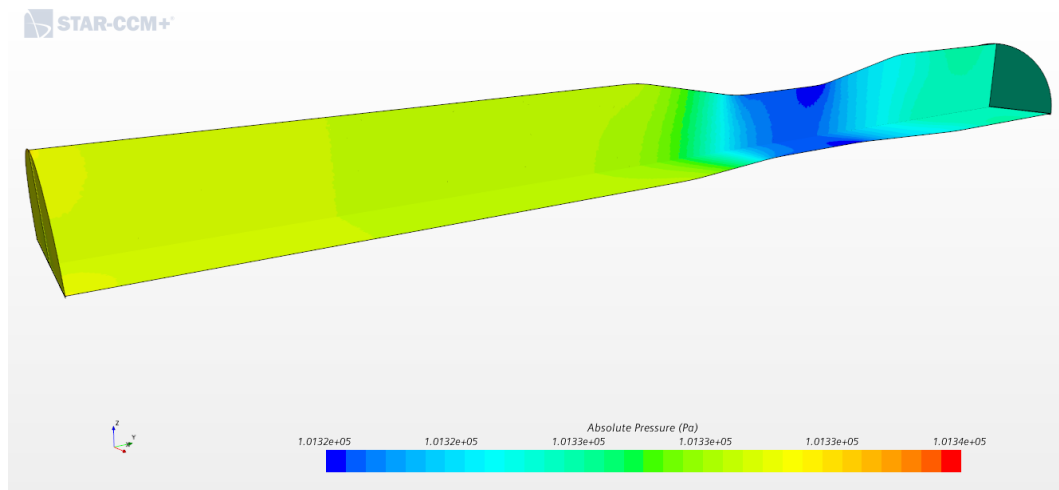


Figure 3.12: Pressure

In the case of velocity, it is seen that air accelerates in the streak. In addition, the presence of a boundary layer on the wall is observed. Upon exiting the striation, the fluid presents inhomogeneities related to the vorticity that accumulates.

Quarter circles are used to highlight the velocity profile and its axisymmetry, which is consistent with the theory.

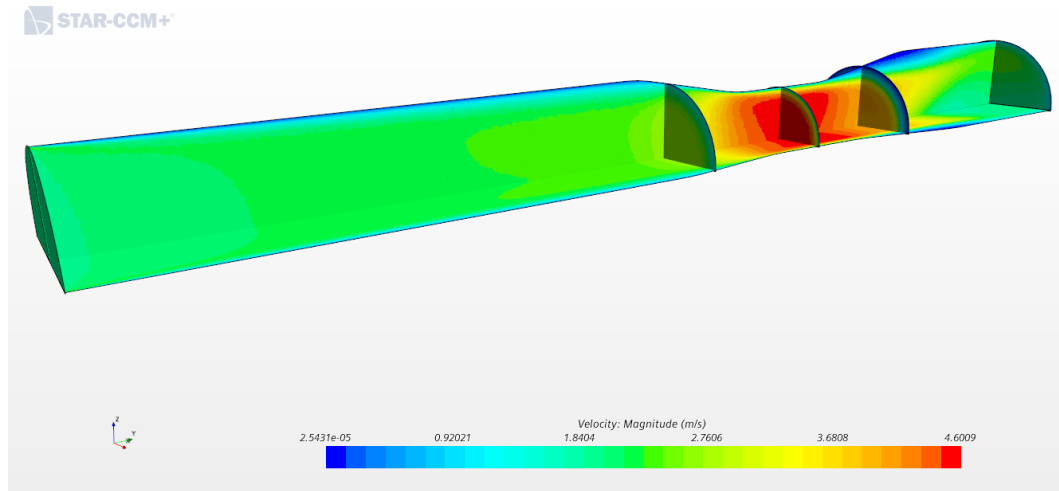


Figure 3.13: Magnitude of speed

In Figure 3.14 it is observed the dual behaviour of velocity and pressure. Moreover, a numerical error can be observed in the upper edge of the input section. Here, the fluid at the edge sees a kind of stopping point and thus sees an almost zero velocity, which is equivalent to the maximum pressure peak considering their inverse proportionality.

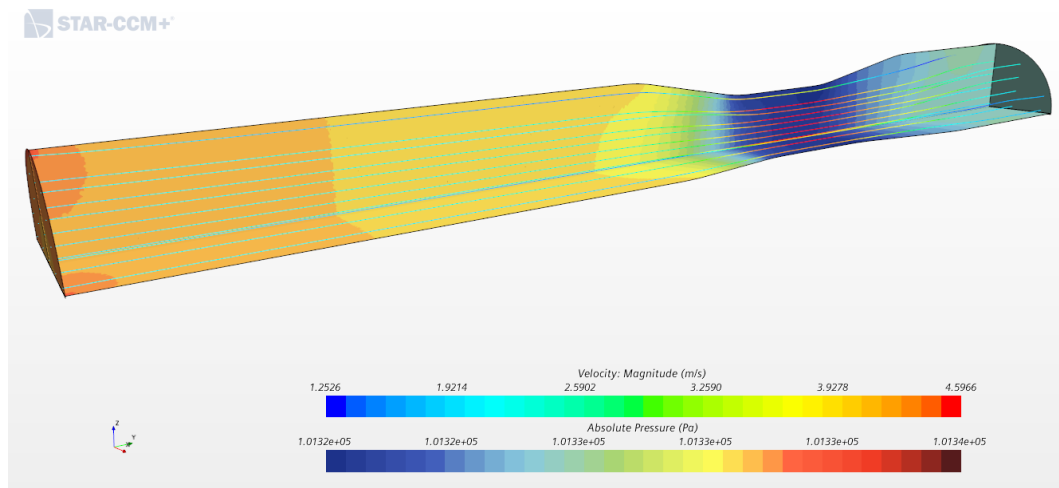
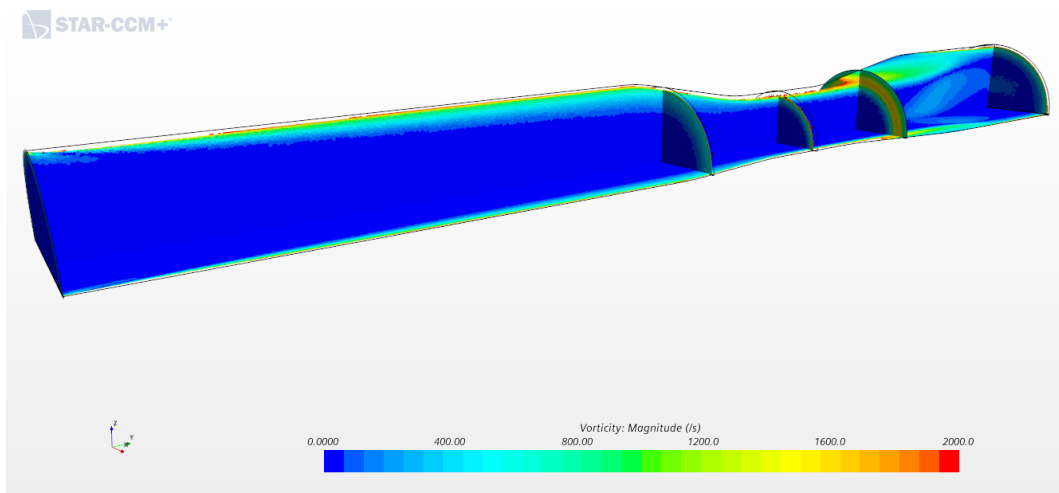


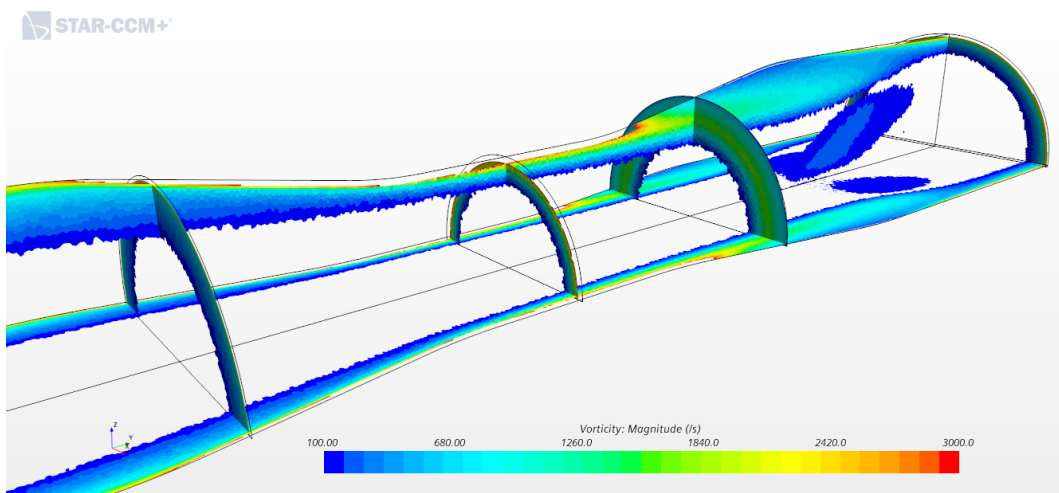
Figure 3.14: Pressure and speed

The vorticity is very low along the entire axis of the duct and increases on the

wall, where you can also notice the increase in the size of the boundary layer as you advance in the stretch of the duct with constant section. It is evident that at the exit of the squeeze, there is a strong increase in vorticity that gives rise to a recirculation zone. Looking at the detail Figure 3.15b we went to cut the lowest values of the vorticity, discarding the values below 100, to highlight the regions where there is a concentration of vorticity relevant unless the walls. In general, near the wall and at the exit of the bottleneck vortices are quite stable.



(a) Overall vorticity



(b) Vorticity detail

Figure 3.15: Vorticity

To see the trend of the variables along the axis line (Probe 1) and along a parallel axis placed at a distance of about 1.5 mm from the wall of the striction (Probe 2), two probe were defined in StarCCM+ probes were defined and used to sample pressure and speed in 1000 points. Probes are a tool for displaying on axes the value of a given variable taken by all cells that are intersected by the same.

The pressure of the two probes is observed. Initially, there is a greater pressure than the environment at the entrance, to allow exhalation. It then decreases due to the physics of the constant section duct, characterized by hydraulic losses, until it reaches the shrinkage where there is a sharp decrease in pressure, which then goes up to the ambient pressure.

Since the pressure is constant along the normal wall, the two probes record practically the same values, but the probe placed closer to the wall follows a more angular trend, probably related to a delay of the pressure signal to rise from the wall to the duct axis.

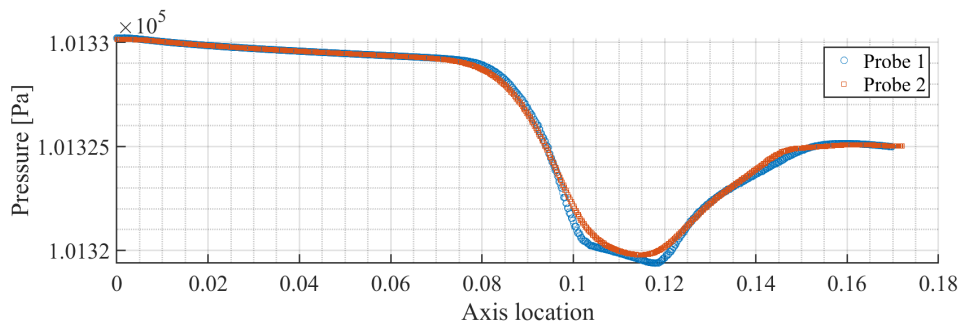


Figure 3.16: Pressure CFD

The velocity seen by the two probes has an inverse trend compared to the pressure seen in Figure 3.16. There is an acceleration in correspondence of the striction, while after it is returned to a speed similar to the initial one (2 m/s), but with a deviation between probes 1 and 2 after the striction. This difference is caused by the presence of the vortex previously indicated.

The 3 components of the speed are represented. In particular, along the z direction probe 2 assumes an almost constant value, instead, the one that is

closer to the duct wall is affected by the change of geometry, assuming constant values in the first initial section, then negative, positive finally return to the initial ones. Concerning the velocity in y direction it has a trend similar to the one of the magnitude of the velocity.

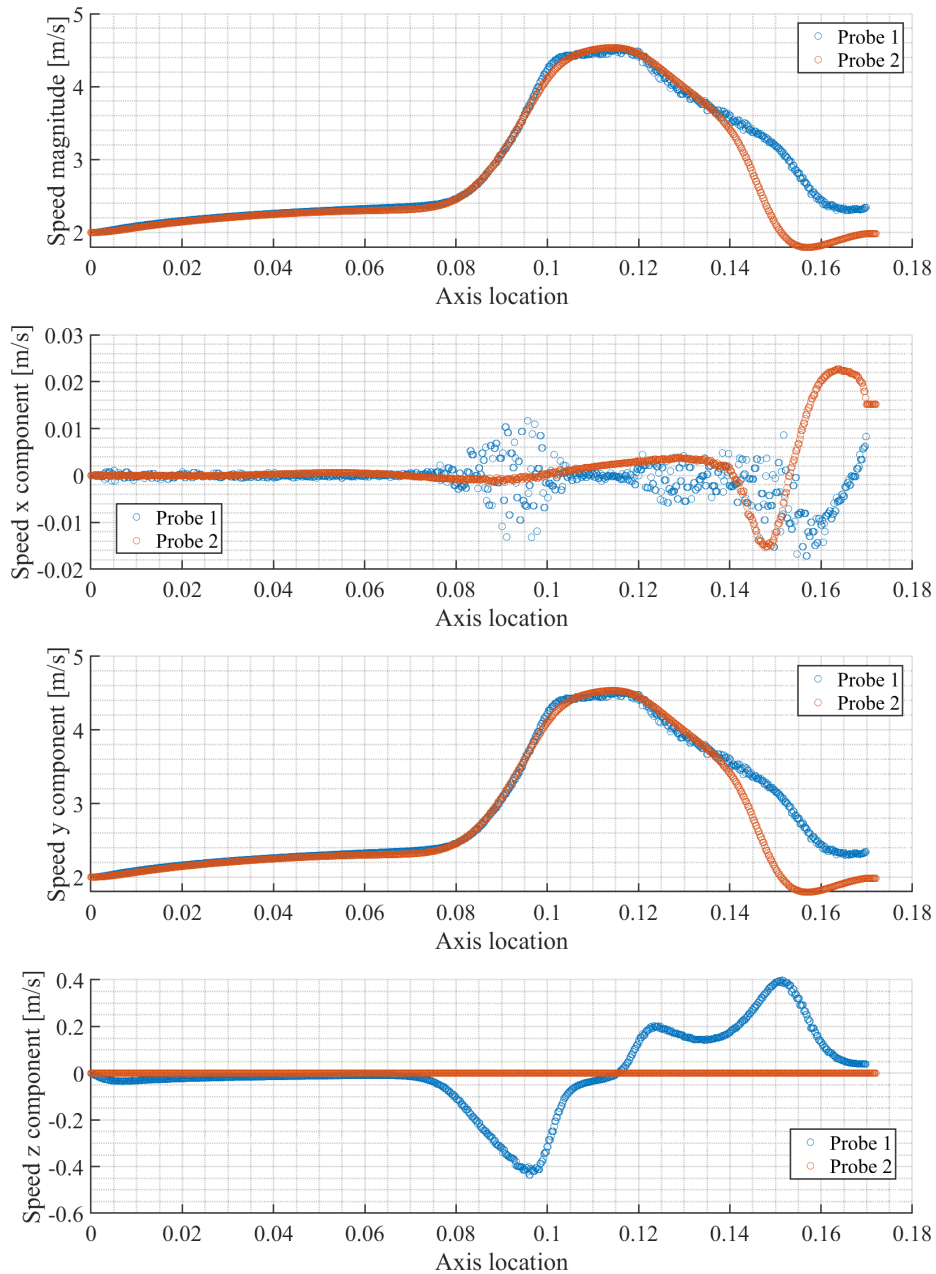


Figure 3.17: Velocity

Finally, we observe the trend of vorticity, it can be seen that it grows in the shrinkage and is greater in the probe placed near the wall because of the

interactions wall-layer boundary and the presence of the vortex downstream of the striction.

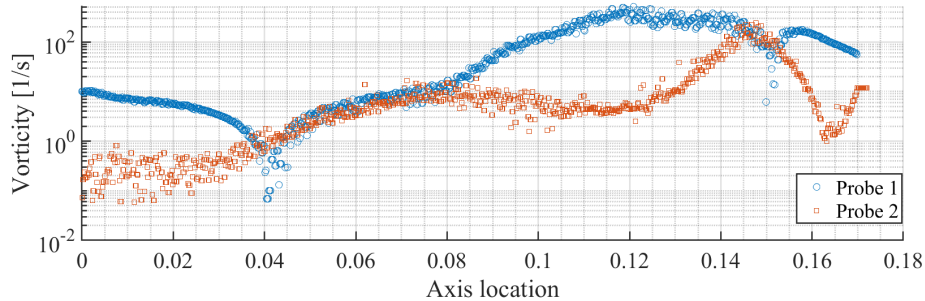


Figure 3.18: CFD vorticity

### 3.3.3. Limitation and approximation

The spirometer designed nevertheless has approximation and limitations.

- In general, the Venturi tube is based on Bernoulli's principle, which, to be valid, needs to be under stationary and laminar conditions.
- No account is taken of the pressure losses associated with an actual duct. Losses only cancel out in the ideal case of an infinitely long duct.
- The treated motion is not developed, one would need much greater venturi lengths

In any case, the next section will compare the sensor with a commercially available spirometer to highlight its validity.

### 3.3.4. Spirometer results verification

The sensor designed during the thesis was compared with a commercially available flow sensor already used for spirometry. To be precise, it was tested with an SFM3400 sensor from Sensirion.

Ten 15-second breaths were taken to correlate the signals. A subject sitting in

a chair with his feet on the floor was asked to take these measurements in a row. The configuration had the flow sensor in front of the differential pressure sensors placed in series so that they would see the same flow.

In the diagram in Figure 3.19, 3 different signals can be seen, the blue dashed signal represents the signal obtained from the flow sensor, while the yellow and red signals are from the differential pressure sensors. It can be seen that the two sensors follow the flow sensor quite closely but alternate in the breathing phases. It can be seen that sensor 1, the one placed near the mouthpiece, follows the inhalation phase well, whereas the second one follows the exhalation phase well.

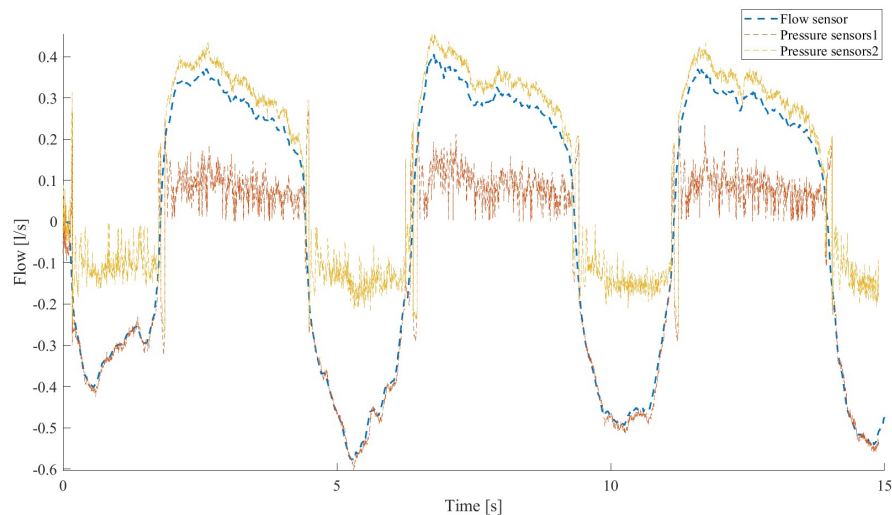


Figure 3.19: Comparison between spirometers

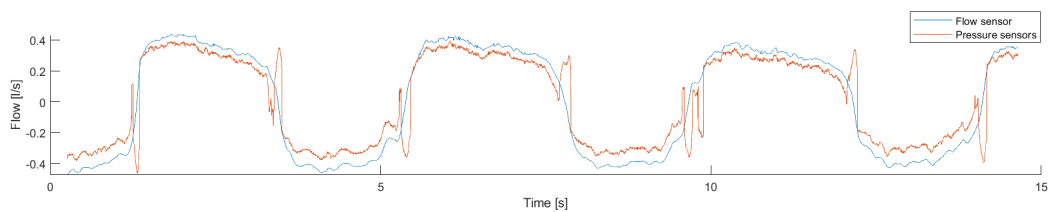
For this reason, it was decided to consider the two signals only when they represent the signal well, i.e. to use the first for inhalation and the second for exhalation. To do this, the difference between the modules of the two pressure sensor signals was made using a sign function.

$$Signal = SP_1 \cdot (sign(|SP_2| - |SP_1|) == -1) + SP_2 \cdot (sign(|SP_2| - |SP_1|) == 1); \quad (3.5)$$

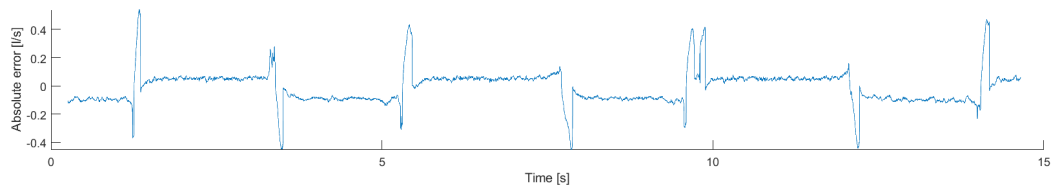
The output of the latter can be 1, -1 or 0, in our case we will only get 1 or -1 as output. If the sign function returns 1 we multiply the signal of the first

sensor by one and 0 by the signal of the second sensor, thus in the inhalation phase, in the exhalation phase exactly the opposite happens. The signal we obtain can be seen in Figure 3.20a.

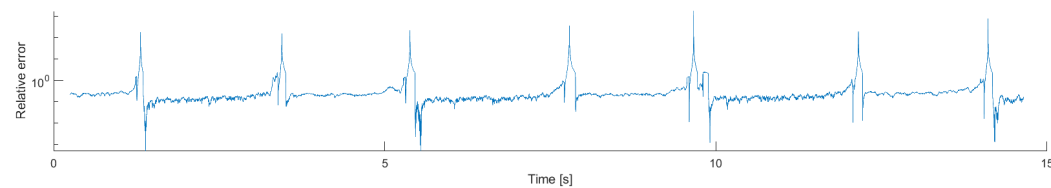
Relative and absolute errors were then calculated. In both cases, it can be seen that they oscillate around zero, except for a few peaks at the transient. This is because pressure sensors, unlike flow sensors, are affected by the transient. The pressure sensor used tends to underestimate the flow, as if there is a bias. This error can be reduced by calibrating with a more accurate instrument, but this was impossible with the instrumentation available.



(a) Total signal



(b) Absolute error



(c) Relative error

Figure 3.20: Signal obtained

Finally, the relative and absolute errors of all ten measurements were plotted in the form of histograms. It can be seen that the average value is almost 0, but errors in the order of 0.4 l/s can occur. Although the probability of having high errors is very low, this may be because, as mentioned earlier, the

pressure sensor is affected by the transient unlike the flow sensor, and the fact that we still have two different sampling frequencies between the two sensors considered.

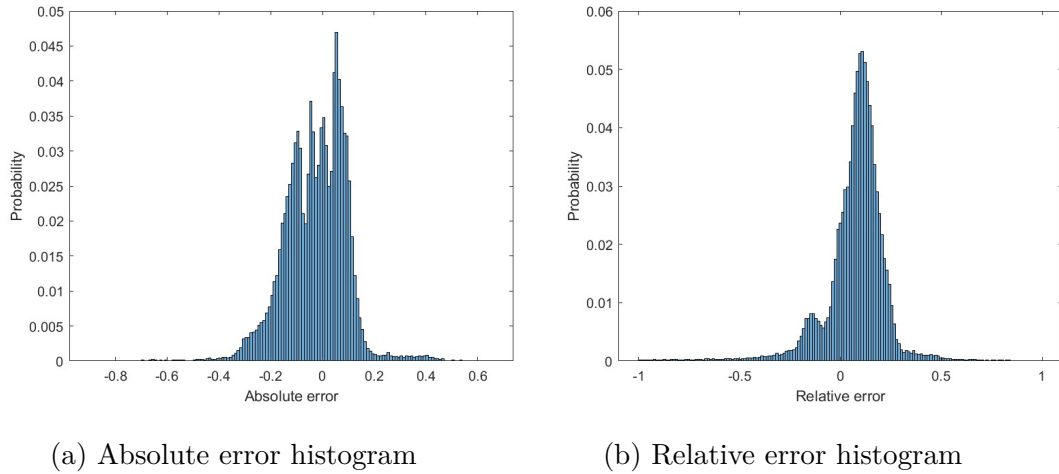


Figure 3.21: Error histogram

Finally, the correlation coefficients between the two signals were calculated for all 10 acquisitions. Averaging this gave a value of 0.9874.

Acquisition	Correlation coefficient
1	0.9962
2	0.9946
3	0.9909
4	0.9927
5	0.9932
6	0.9924
7	0.9930
8	0.9901
9	0.9490
10	0.9817

Table 3.1: Correlation

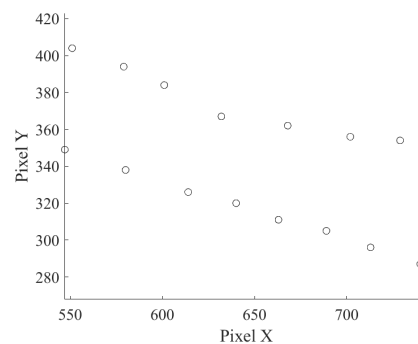
## 4. Methodology and protocol

The diameters, calculated in each frame, have been used to evaluate the CI. To do so, it has been selected 8 points on the upper side and 8 on the lower side of the vein to obtain 8 diameters per frame (4.1a). It was not possible to evaluate each frame so it has been selected only some frames with a pitch of 5. Each video analysed is composed of 299 frames, so it has been possible to evaluate  $\sim 60$  frames per video.

The points selected in the video are then represented on the vein. (4.1b) After picking the points, an algorithm has been implemented to calculate the 8 diameters. It has been used two third-order interpolating polynomials for both the points above and below, of the two functions obtained I take an average in this way it is possible to obtain the middle dashed line. 4.2a is calculated as the derivative, and thus the slope of the line, at 20 points, it is then calculated the perpendicular lines to calculate the diameters by finding the intersection points. To find the intersections between the two polynomial functions and the perpendicular lines, the method of **Newton-Rapson** has been used.



(a) Segmented vein



(b) Points on the vein

Figure 4.1: Vein

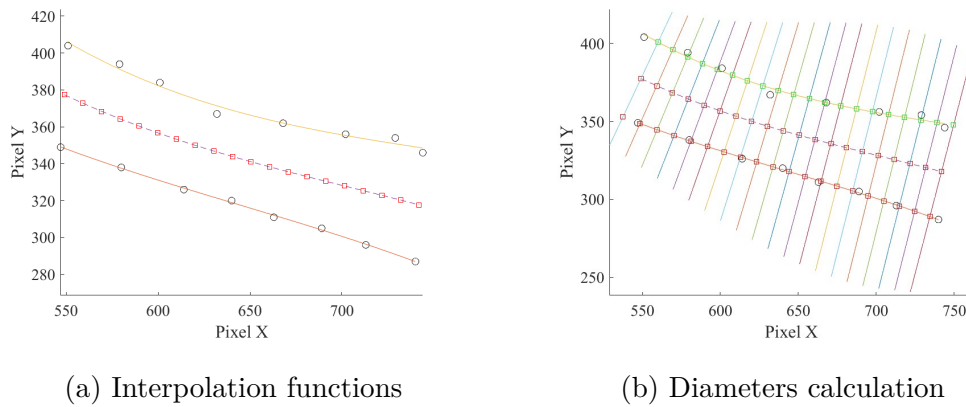


Figure 4.2: Vein

After having calculated 20 diameters at each frame it has been possible to evaluate mean and standard deviation. At the first moment, the mean of the 20 diameters was used as the diameter of each frame, but this gave some problems with random spikes. To overcome this problem it has been used hydraulic diameter, it helps to consider a non-circular duct as a circular tube by converting the cross-sectional area to a circular one. Indeed it was seen as a more reliable and physiological trend.

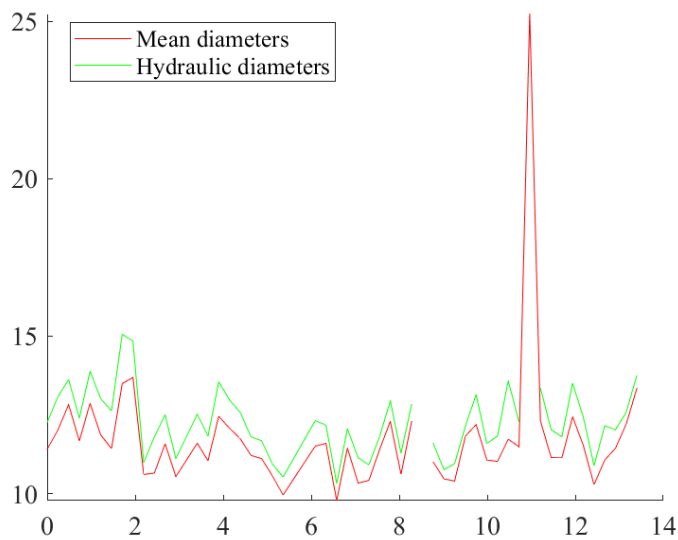


Figure 4.3: Difference between mean diameters and hydraulic diameters

## 4.1. Protocol

In this master thesis has been analyzed a person with an age of 23.

The acquisition has a duration of 30 minutes in which are required 5 types of measurements repeated twice. The subject is placed in a supine position on a medical bed during which, while breathing into the spirometer, an ultrasound scan of the abdomen is acquired. The ultrasound scanner was used in the same way, which means that the mark on the probe was positioned upwards. The probe was placed next to the navel on the right side of the abdomen. In order to obtain the most precise acquisitions possible, the probe was never lifted from the patient's abdomen to try to minimise as much as possible the variations in diameter due to the different anatomy of the tract analysed, to assess only those of interest to us, namely those due to the heartbeat and breathing. The inferior vena cava does not present a perfectly cylindrical geometry but tends to vary its diameter along its length.

The five types of measurements performed are

- First: Normal breathing for 20 seconds with the spirometer
- Second: Normal breathing for 20 seconds with the spirometer and the tap water
- Third: Forced breathing for 20 seconds increased by 5% compared to normal breathing, both in inspiration and exhalation, with a spirometer and tap water
- Forth: Normal breathing for 20 seconds with the spirometer and the tap water with leg raised
- Fifth: Forced breathing for 20 seconds increased by 5% compared to normal breathing, both in inspiration and exhalation, with spirometer and tap water and leg raised

For the third and fifth acquisitions, the increase was calculated from the first type and represented on screen in real time to allow the subject to see it and exceed it.

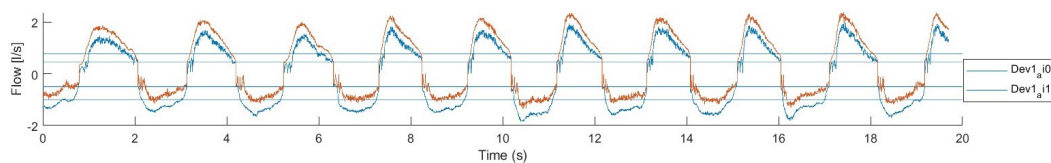


Figure 4.4: Acquisition with increased bands

After each type of acquisition, the subject was given about one minute's break. Indeed, before performing the two tests with the legs raised, which means the fourth and the fifth type of acquisition, the subject was asked to raise his legs 50 cm for about 3 minutes, to permit an increase in pressure and thus to be able to perform the measurements under the hypothesised conditions.

## 5. Results analysis

In this section, a 23-year-old non-smoking woman with a weight of 60 kg, will be examined in detail as a case study.

### 5.1. First type of acquisition

In the first acquisition, there is the measurement of normal breathing carried out for a time of 20 seconds in the spirometer. The diameters obtained by manual segmentation using Viper are loaded and the previously calculated hydraulic diameters, are interpolated to obtain a trend. The standard deviation on the average diameters is also calculated to highlight the fact that they are not exactly reliable, considering the huge variation of their standard deviation. The first step is to filter the flux signal to make it smoother with an implemented Matlab function **smoothdata** whose parameters entered are: Gaussian filter on a window with a length of 500.

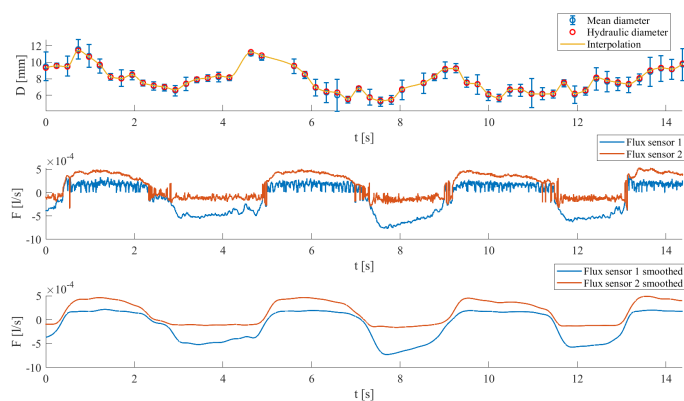


Figure 5.1: Relation between flux and diameters

As it can be seen in Figure 5.1, a correlation between flow and diameters can be observed, however slightly delayed. As expected from theory, a decrease in

the diameter of the vena cava should be observed during inspiration. Instead, during exhalation the exact opposite should occur, an increase in the diameter of the vein.

To further emphasise this correlation, the PSDs of the three signals (spirometer and two sensors) were made. As can be seen, all three have a peak at a frequency considered to be the respiratory rate, whereas only the PSD of the diameters gives another peak at the cardiac rate. The first picture represents the PSD on a logarithmic scale.

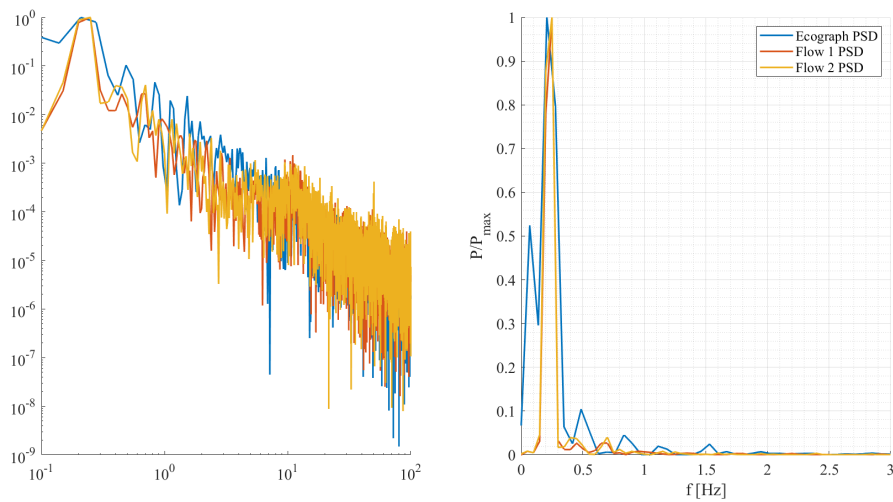


Figure 5.2: Correlation of PSD

Then, observing the very fast variations of the signals, it was decided to evaluate the variation of the diameters due to the heart rate and that due to the respiratory rate to eliminate oscillation frequencies that were too high to be considered physiological. The frequency has been selected manually on the PSD of the signal. As it can be seen by Figure 5.3 in this type of measure respiratory rate has a greater impact in this type of measurement.

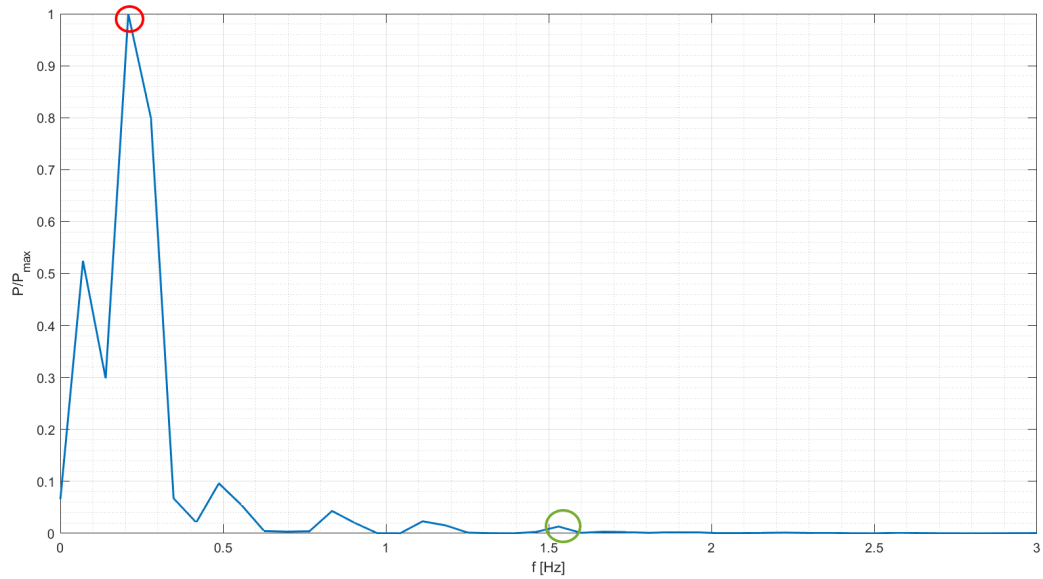


Figure 5.3: PSD of the diameters

Considering that the heart rate is higher than the respiratory rate, a double-pass low-pass Chebychev filter was implemented on Matlab with a cut-off frequency equal to the heart rate increased by 0.2Hz, and it ends up cutting at a frequency also equal to the heart rate but increased by 0.7Hz.

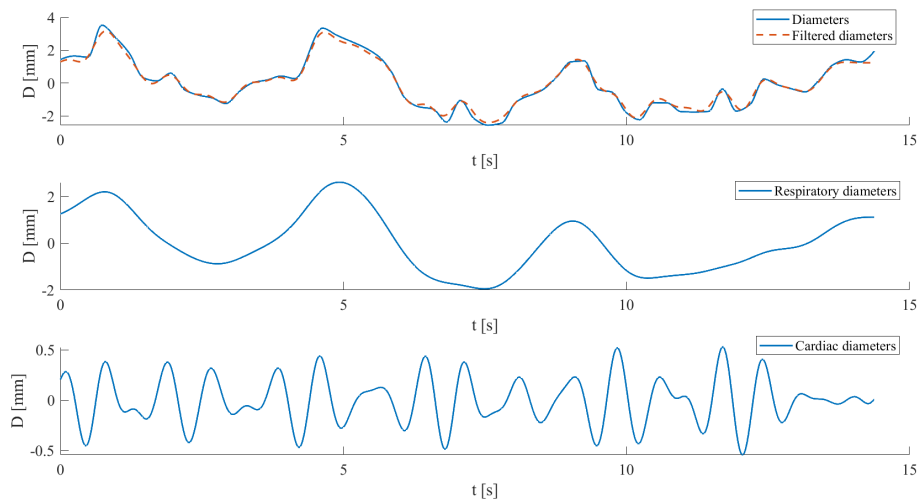


Figure 5.4: Filtered diameters

Similarly, two other filters were implemented to be able to assess changes in diameters due to heartbeat and respiration separately.

For the former, a high-pass filter was implemented with a cut-off frequency equal to the heart rate decreased by 0.5Hz and an effective start of the pass band at a frequency equal to the heart rate decreased by 0.25Hz.

For the second, a low-pass filter was used with a cut-off frequency equal to the respiratory frequency increased by 0.2Hz and end of cut-off at a frequency equal to the respiratory frequency but increased by 0.7Hz.

The spirometer, designed as described in the previous chapters, has a millisecond resolution, whereas the ultrasound scanner has a resolution of seconds; in addition, the ultrasound scanner took measurements of 14 seconds, thus cutting 6 seconds off the spirometer's measurement. To try to solve this problem, and thus to try to make the two signals synchronous, it was decided to calculate the correlation between the two signals for several delays between the two, to assess the actual delay and thus position them correctly, since for each measurement the delay could change slightly.

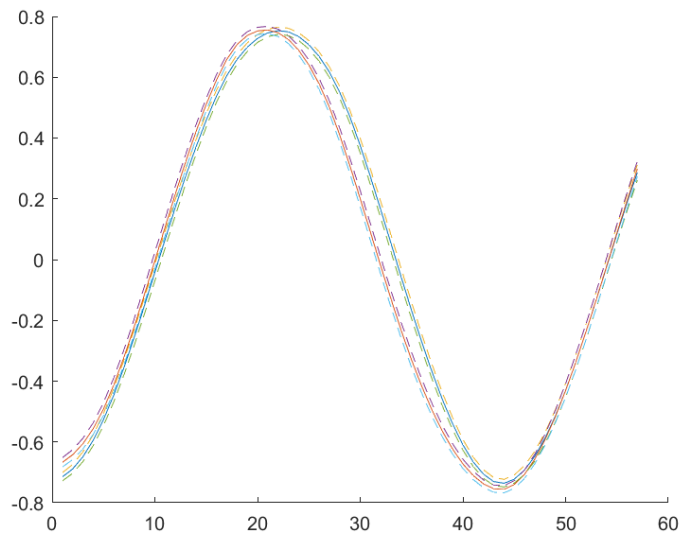


Figure 5.5: Correlation function for delay

As can be seen by the figure, in this case, the correlation among the signals is maximum at a delay of 2.1 seconds.

Realigning the two signals shows a higher correlation than at the beginning.

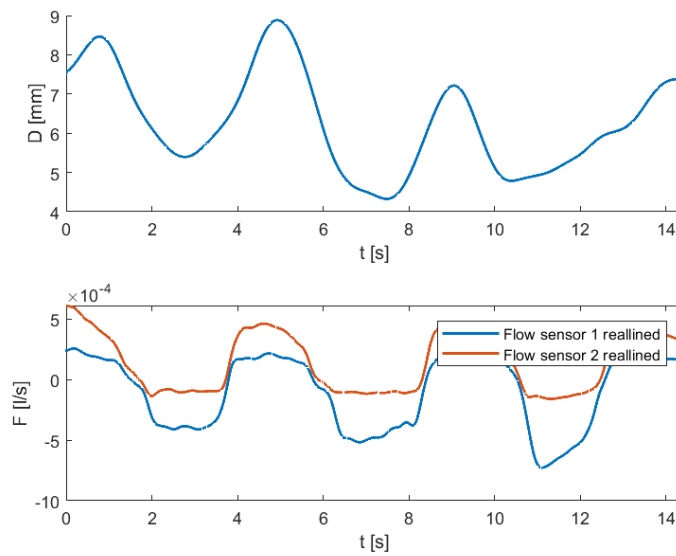


Figure 5.6: Correlation function for delay

About this type of measurement, it remains to analyse the caval index, namely the total caval index, the cardiac caval index (CCI) and the respiratory caval index (RCI). [10]

The formula utilized to calculate the caval index is:

$$CI = \frac{D_{MAX} - D_{MIN}}{D_{MAX}} \quad (5.1)$$

In which  $D_{MAX}$  is the maximum diameter registered during exhalation, while  $D_{MIN}$  is the minimum diameter registered during inspiration, both calculated in the same respiration cycle.

CCI and RCI are calculated in the same way as the CI, but, while the caval index considers the totality of diameter variations, following the first filter which eliminates non-physiological variations, the other two are calculated in different cases. To be precise, the first, namely the cardiac one, is calculated on the variation of diameters due only to the heart rate, while the second is calculated on the diameters filtered so that there are only the variations due to breathing.

In this specific case, the values calculated are:

Acquisition	CI	CCI	RCI
First	55%	19%	51%

Table 5.1: Caval index first acquisition

As it can be seen by Table 5.1 the CI is bigger than the other two, and the Cardiac Caval Index is smaller than the respiratory one. This was also expected when looking at the PSD one could see the different peak heights.

## 5.2. Second type of acquisition

The second acquisition is characterised by the measurement of normal breathing carried out for a time of 20 seconds in the spirometer plus the tap water. This kind of test has been carried out to induce greater muscular effort as the added tap has a very small bottleneck the ratio of the areas of the spirometer is 2.04, while the one of the tap is 6.25.

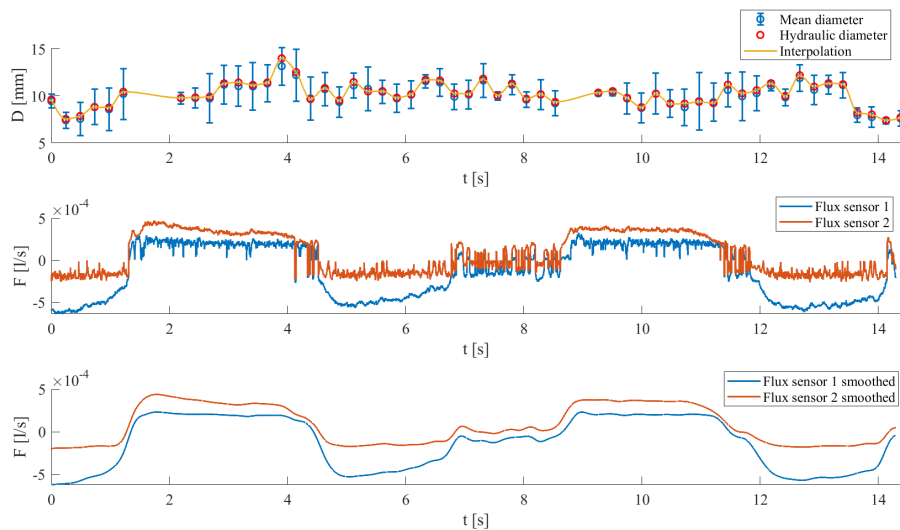


Figure 5.7: Relation between flow and diameters with tap

Even in this case, it can be seen a slight correlation between the variation of the diameters and breathing. This can be used in the PSD to underline the correlation between these two factors.

Peaks are not completely coincident, but are separated by a slight gap, probably caused by manual segmentation.

When, as in this case, there are many close peaks at the respiratory frequency, and it is difficult to choose the right one, one relies on the PSD of the spirometer and selects that as the respiratory frequency, but considering that it is almost at the middle between two spikes, it is chosen the one with bigger frequency.

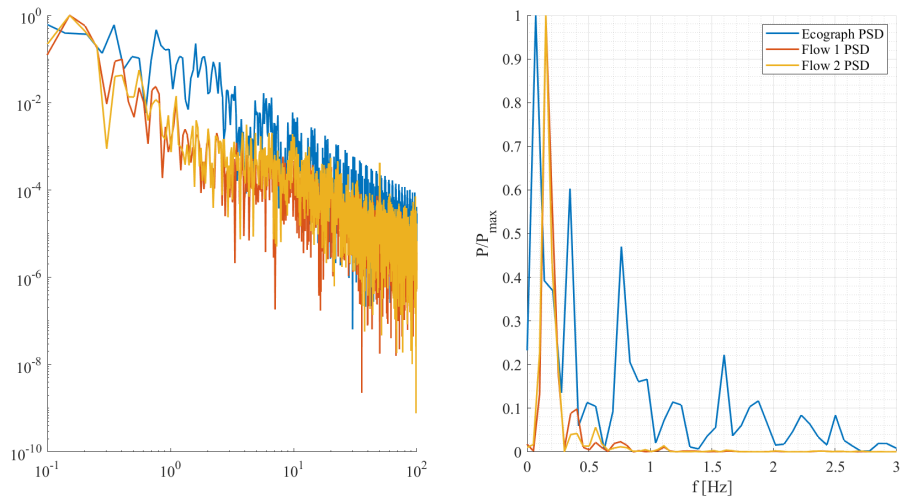


Figure 5.8: PSD in the measure with tap

In this case, unlike in the previous case, the heart rate is evident. After having examined the PSD, there has been implementation of filters to evaluate separately the caval index. Even in this case, it is possible to represent the two trends separately.

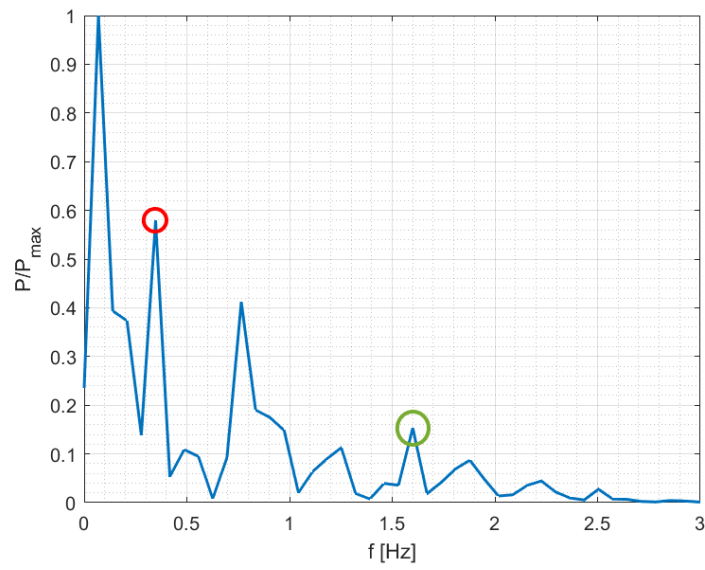


Figure 5.9: PSD with diameter with tap

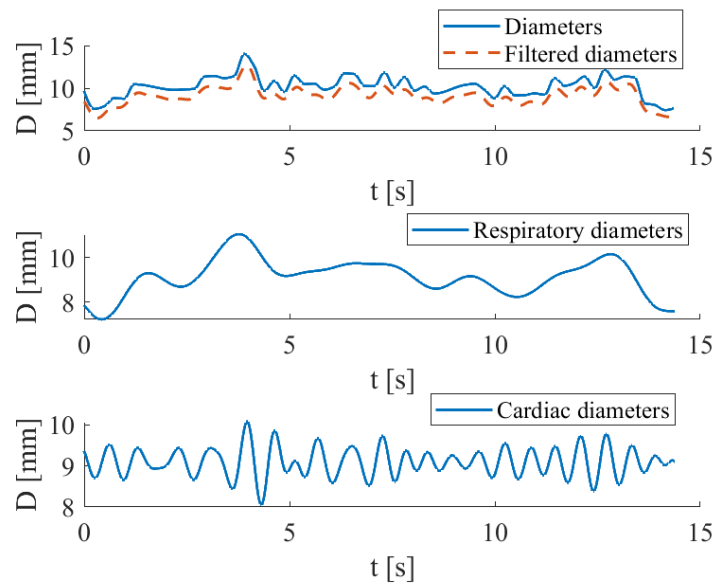


Figure 5.10: Variation of diameters with filters

As mentioned in the previous paragraph, the delay between the two signals is not always the same it has been calculated using a correlation function and it can be seen that in this case, it coincides with 0, exactly where it can be found the maximum peak.

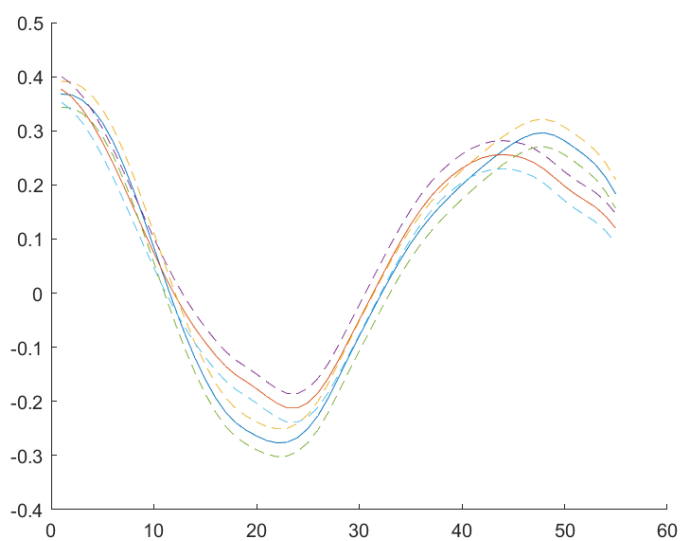


Figure 5.11: Correlation function for delay with tap

Realigning the signals results in this trend

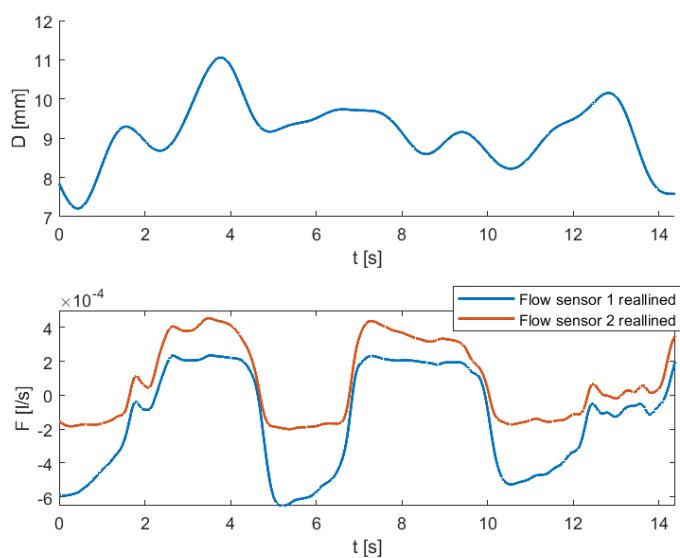


Figure 5.12: Allined signals with tap

The three Caval Indexes obtained by these measures are a bit smaller than in the previous case.

Acquisition	CI	CCI	RCI
Second	48%	16%	34%

Table 5.2: Caval index second acquisition

### 5.3. Third type of acquisition

This third type of acquisition is still characterised by the use of the tap, but in this case, the subject is asked to exceed thresholds in both inhalation and exhalation, which are increased, in comparison to the first measure, by 5%, with the duration of 20 seconds.

After having filtered the signal, it can be visualized the trend of the diameters and the spirometry.

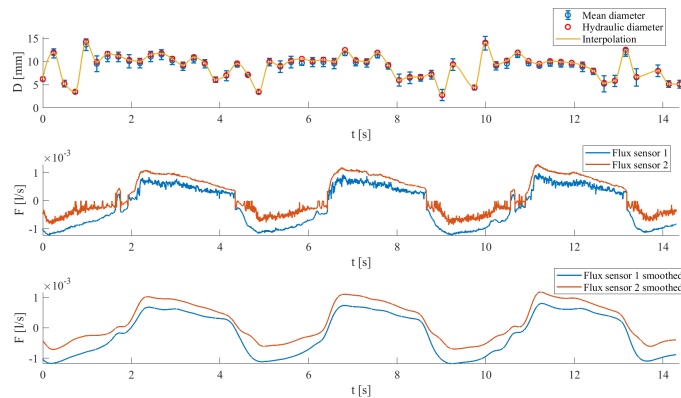


Figure 5.13: Diameters with augmented amplitude

From PSD it can be seen that the peaks of respiratory frequency are perfectly overlaid, this underlines the correlation between the two signals.

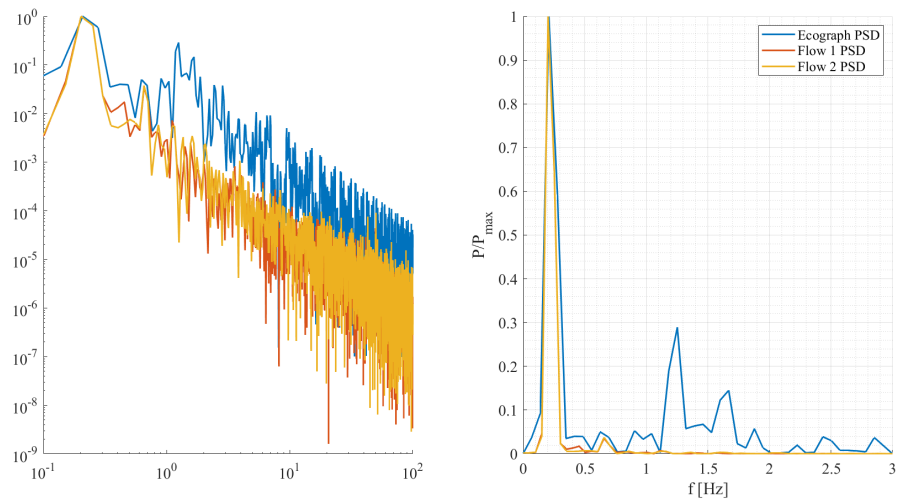


Figure 5.14: PSD in the measure with tap and augmented amplitude

Considering the presence of only one peak it has been easy to pick the respiratory rate and the cardiac frequency.

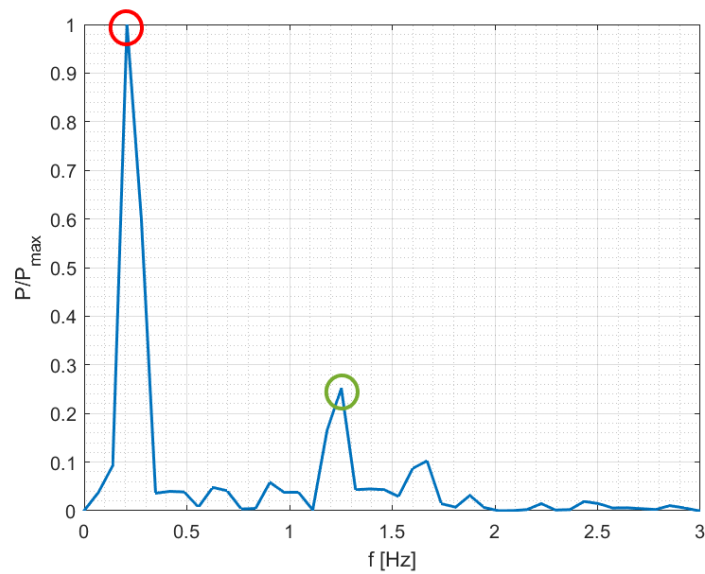


Figure 5.15: PSD of diameters with augmented amplitude

Variations in diameters due only to the frequencies of interest, i.e. respiratory and cardiac frequencies, can also be represented.

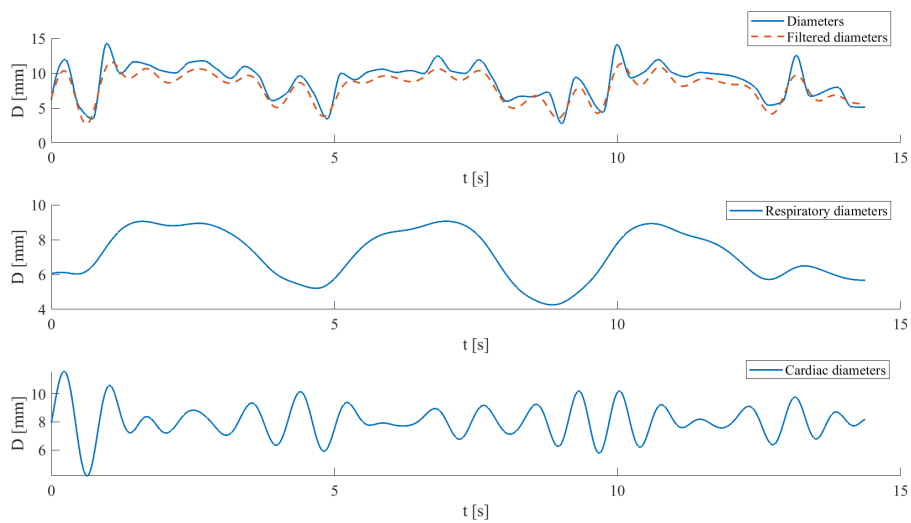


Figure 5.16: Diameters with augmented amplitude

In this acquisition, there is a delay of 1.8 second.

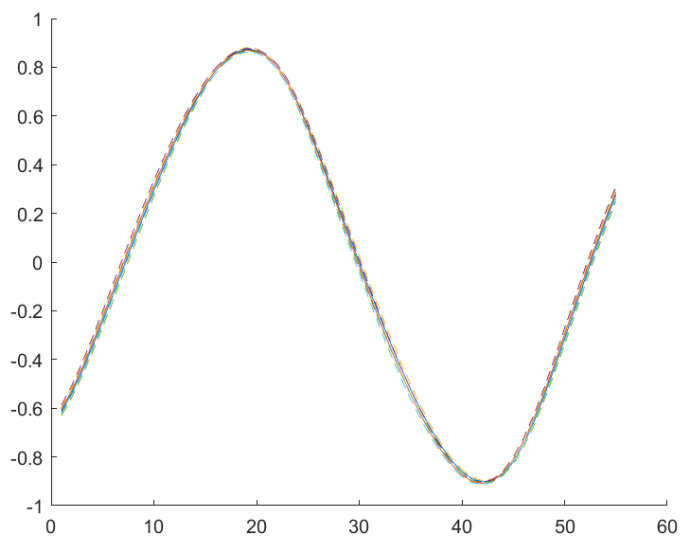


Figure 5.17: Delay for the measure with augmented amplitude

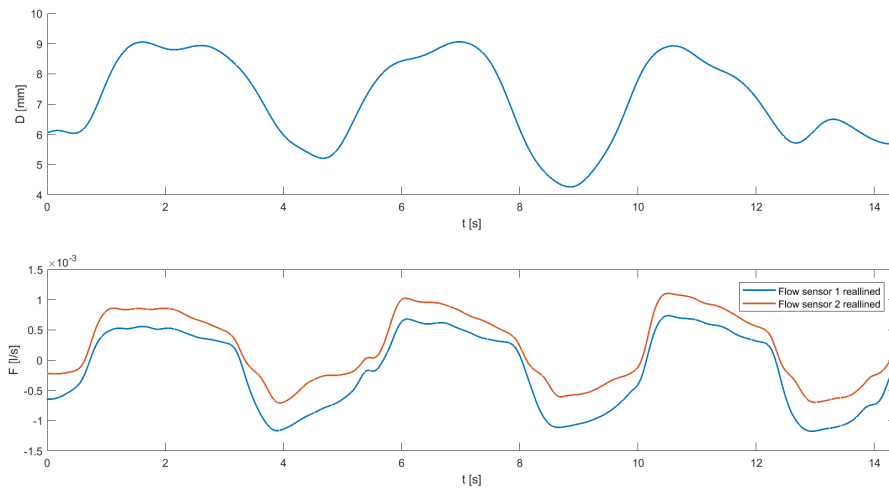


Figure 5.18: Allined diameter for the measure with augmented amplitude

The aligned signals show a very similar pattern to each other. As expected, given an induced strain on the patient, the vein responds with increased collapse and thus increased caval index.

Acquisition	CI	CCI	RCI
Third	76,8%	64%	53%

Table 5.3: Caval index third acquisition

## 5.4. Fourth type of acquisition

For the fourth type of measurement, the subject was asked to raise his or her legs about 50 cm on support. This is done starting 3 minutes before the acquisition, to ensure a more homogeneous increase in venous pressure. After that, the subject is asked to breathe normally for 20 seconds, without any other further indication.

In previous cases, it has been represented by the variation in the diameter of the vein and the spirometry.

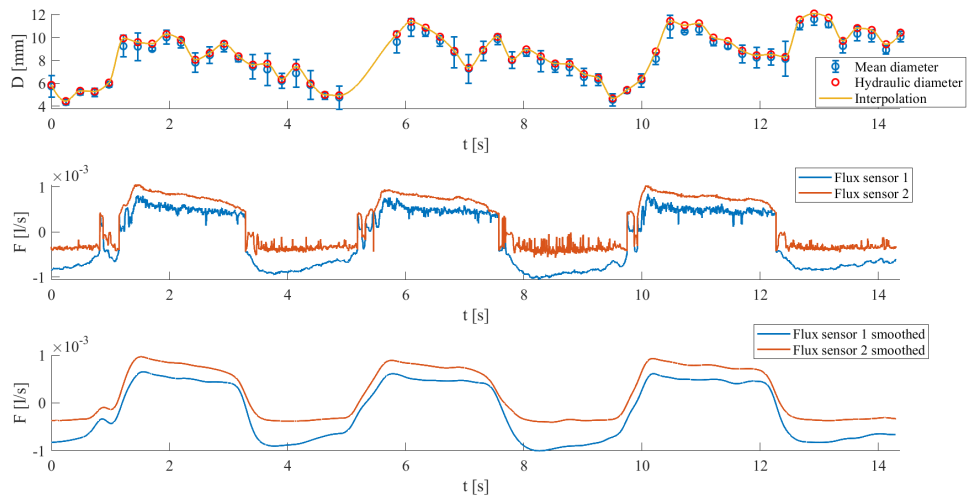


Figure 5.19: Variation of diameters with spirometry

Even by PSD, it can be seen a correlation between the variation of the diameter and spirometry, there is an almost coincident peak.

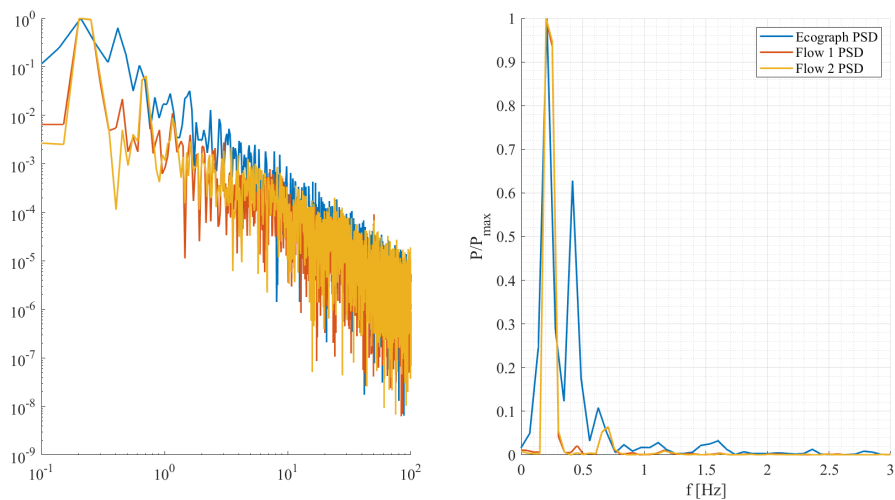


Figure 5.20: PSD of spirometry and diameters variation with raised legs

In this case, the energy under the peak of the cardiac cycle is very low, it is almost hidden, while the one of spirometry is high.

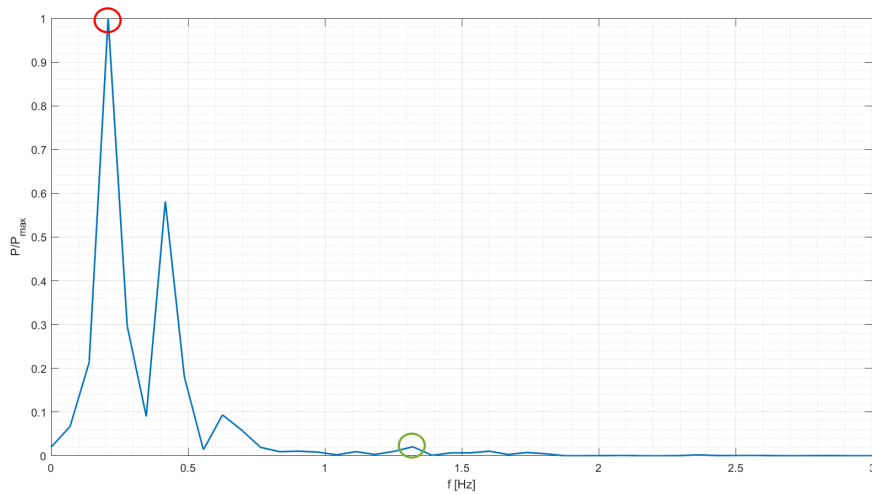


Figure 5.21: PSD diameters variation with raised legs

Figure 5.22 represents the variation of the diameters after having used filters to isolate only the wanted frequencies.

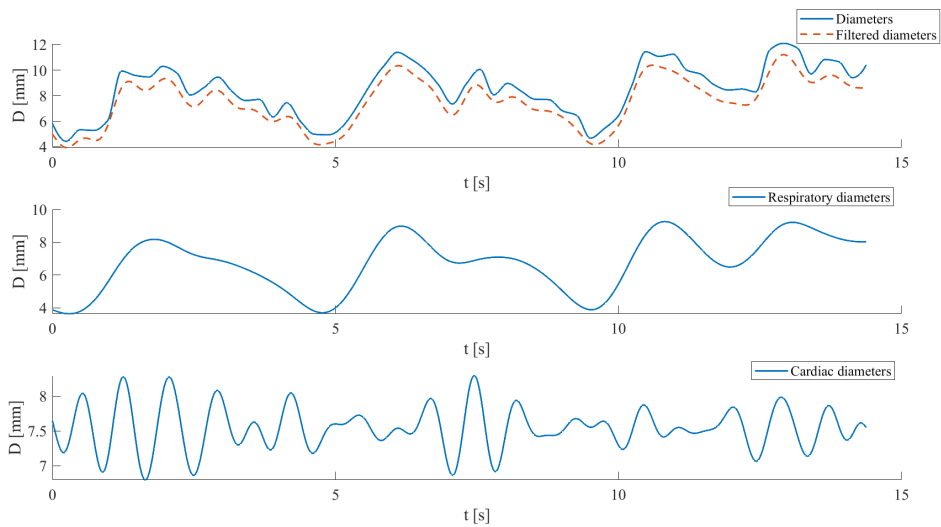


Figure 5.22: Variation of filtered diameters

The delay calculated is quite high, over 5 seconds

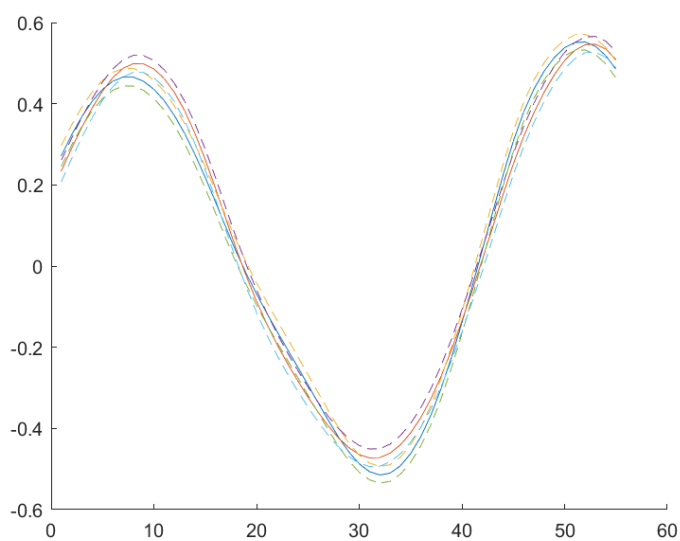


Figure 5.23: Delay between diameters variation and spirometry

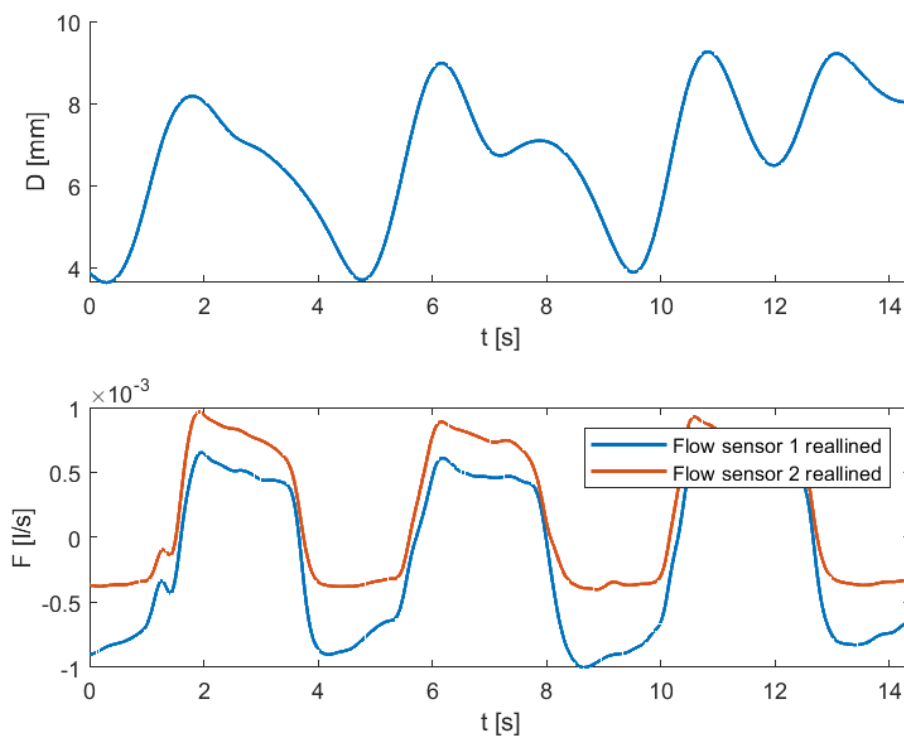


Figure 5.24: Allined diameters with raised legs

Acquisition	CI	CCI	RCI
Fourth	64,9%	18%	60%

Table 5.4: Caval index fourth acquisition

## 5.5. Fifth type of acquisition

In the last type of acquisition, the subject is asked to raise his leg and to breathe for 20 seconds going beyond the limits imposed on the screen, which are equal to the ones present in the third acquisition.

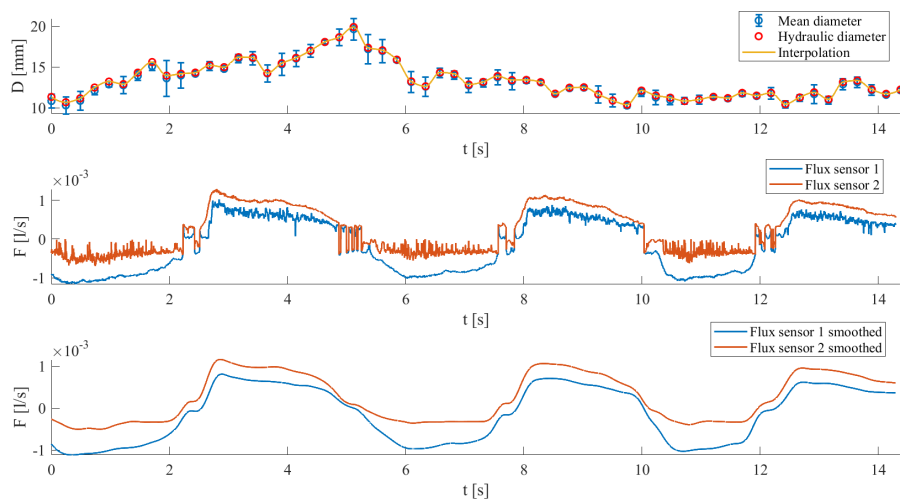


Figure 5.25: Variation of diameters with spirometry and augmented amplitude

The peak of the respiratory rate in the PSD of the three signals is slightly different, an error most likely due to a greater pressure variation within the vein due to the raised legs and possible manual segmentation presenting some error.

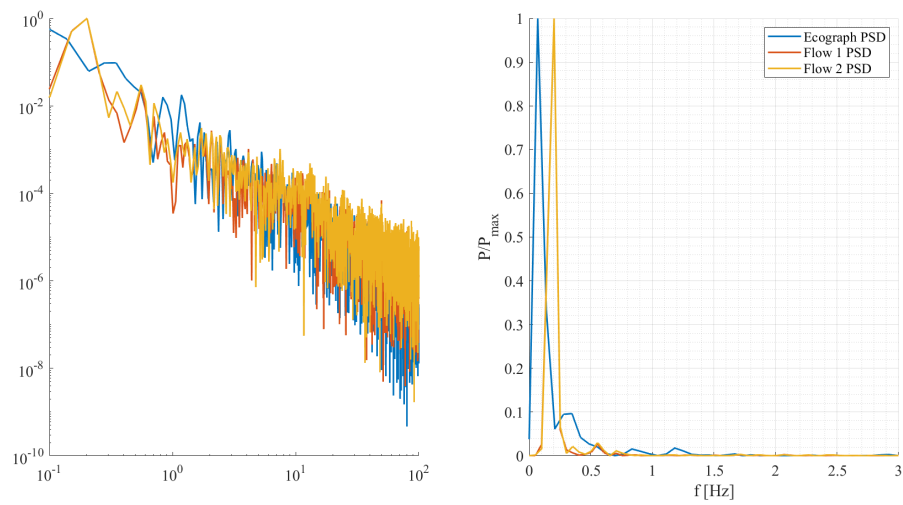


Figure 5.26: PSD of diameter variation and spirometry with leg raised and augmented amplitude

In this case, the heart rate has a very low peak and thus has little influence on the change in diameter, this is caused by the increase in venous pressure and thus the vein has more difficulty in closing and reopening due to the heartbeat alone considering a greater internal resistance given by the pressure.

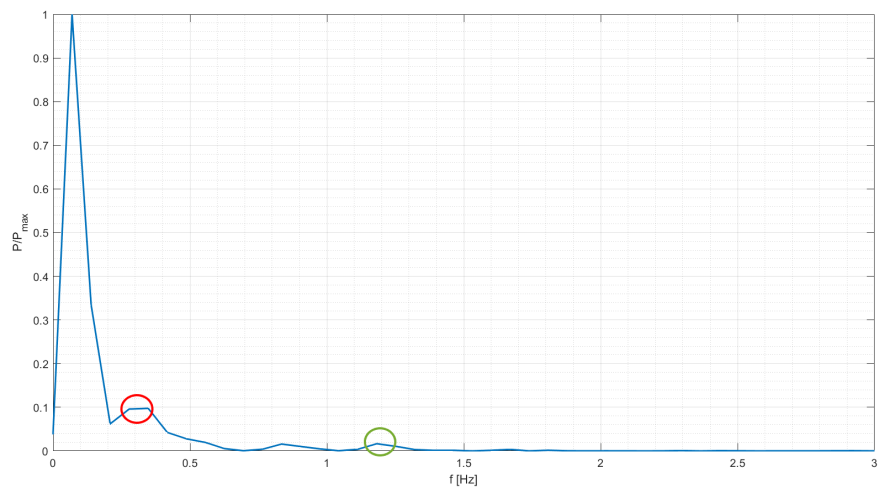


Figure 5.27: PSD of diameter variation with leg raised and augmented amplitude

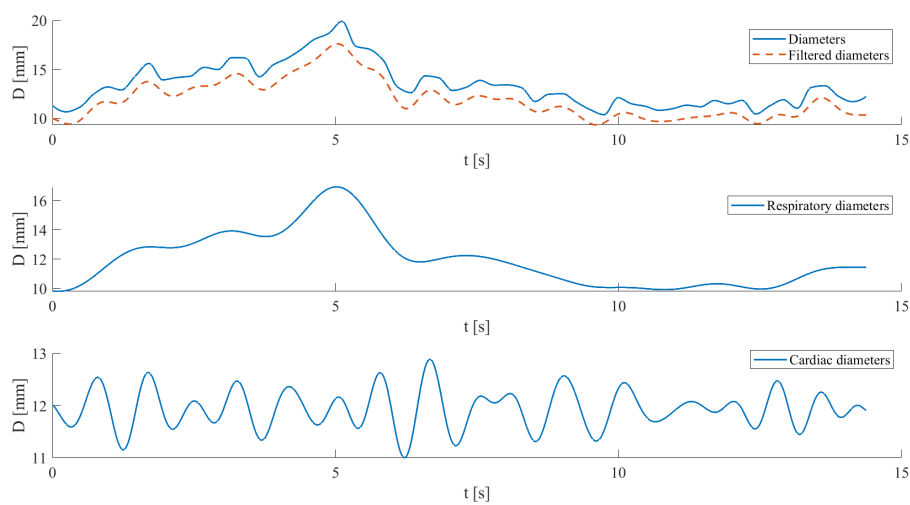


Figure 5.28: Variation of diameters filtered

It can be seen, by the correlation function, a delay of 5.2 seconds.

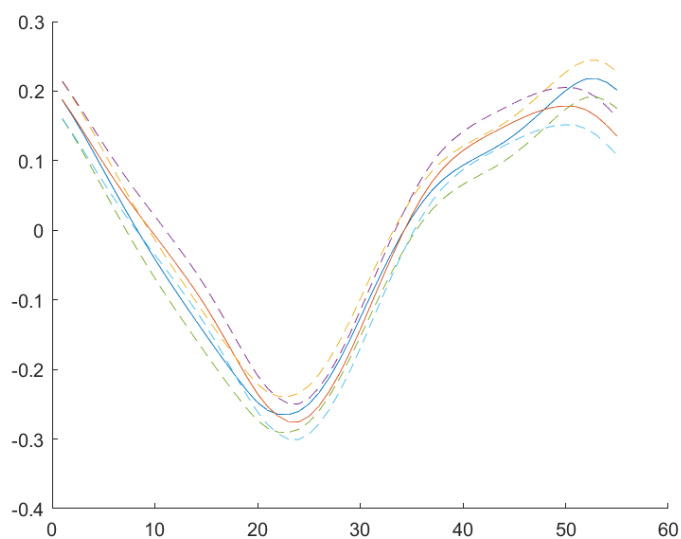


Figure 5.29: Delay of diameters variation and spirometry

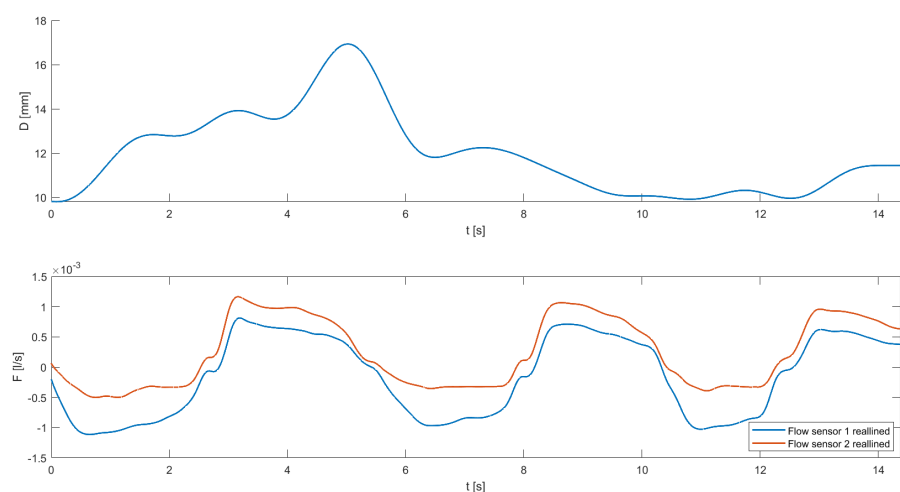


Figure 5.30: Allined diameters with raised legs and augmented amplitude

Finally, you see the three caval indexes calculated. As expected from the previously commented graphs, the caval index is very low. In general, the caval index is not very high as a value.

Acquisition	CI	CCI	RCI
Fifth	46%	13%	43%

Table 5.5: Caval index fifth acquisition

## 6. Discussion and future developments

In this section it will be discussed the results, presented in the previous chapter, and the feasible application of this method.

This thesis aimed to find a way to use a low-cost spirometer in the hospital to help clinics evaluate the status of RAP. Normally, the technique known as 'sniff' is used with the evaluation of the diameter, in which the patient is asked to take a very strong inhalation through the nose to see the change, and thus narrowing of the vein, to calculate the CI. [11] The problem with this technique, which is normally used in hospitals, is that it is not standardised; it depends very much on the patient's ability to breathe in a given way and his cooperation with the doctor, which is not always guaranteed.

For this reason, this thesis sought a method, to be used alongside the sniffing technique, to measure patients' caval index without making it difficult or too patient-dependent. The idea is to induce a muscular effort in the patient so that the vein can increase and decrease in diameter more, obviously, it must be feasible on all patients. The idea was to help the patient in this task by making it visible on the screen in real-time during spirometry. This helps both the subject and the doctor if what is required to make a correct clinical assessment, has been done.

As was mentioned in the previous chapter, a 20-second acquisition was made. However, it was found in post-processing that the ultrasound duration was instead 14 seconds, thus 6 seconds were cut off. The accuracy of the pressure sensor is in the millisecond range, whereas that of the ultrasound scanner is

in the seconds range. To make the two different signals synchronise as well as possible, it was decided to use a correlation function that could find the exact delay of the two signals at the maximum correlation value. It has been evaluated a delay between 0 and approximately 5 seconds, per each acquisition.

Acquisition	CI	CCI	RCI
First	55%	19%	51%
Second	48%	16%	34%
Third	76,8%	64%	53%
Fourth	64,9%	18%	60%
Fifth	46%	13%	43%

Table 6.1: Caval index of the acquisitions

As can be seen by Table 6.1, CI tends to increase as the effort increases. In the first case, there are minor caval indexes, as no effort is required of the patient. It can be seen that the variation in diameter is more influenced by breathing than by heart rate, with a value of 51% compared to 19%. This is because the pressure inside the veins is low, which is why the pulse has little effect.

In the second acquisition, a decrease in all three caval indexes can be observed, especially the respiratory one. This could be because no constraint was given to the patient in this type of acquisition. Furthermore, looking at the PSD of the variation of the diameters, it can be observed that there is not a single peak as far as respiration is concerned, thus there is a less specific energy distribution, which is not observed in the first type of acquisition. This could be due to sub-optimal segmentation or breathing that is not very constant, in any case, it is the breathing that has the greatest influence on the CI.

The maximum value is reached during the third acquisition, in which the patient must exceed the thresholds imposed by the addition of the tap. A

noticeable increase in the Caval Index can be seen, synonymous with the fact that even with low thresholds, the effort induced is sufficient to make the vein and its diameter vary more. In this case, the peak of respiration is well evident and coincides with that of the spirometer. The cardiac peak is also clearly visible. In this case, it can be seen a huge increase in the CCI, which becomes bigger than the respiratory one.

In the fourth and fifth tests, legs raised to increase venous pressure are considered. As a result, the veins are fuller, and thus larger in diameter, and with increased internal pressure. This leads to a decrease in the caval index, especially the cardiac one as it is given by the pulsatility of the vein. The respiratory caval index does not decrease as there is still a muscular effort to breathe, increased by the raised legs, this leads to a greater crushing of the vein during inhalation. In the last case, there is again a decrease in the indices. Another important parameter to evaluate is the variation in the maximum and minimum diameter of the five acquisition types. Indeed, as it can be seen by Table 6.4 the maximum diameter is reached in the last acquisition and the lower is reached in the third. This means that, to evaluate CI it is better to use the third type.

Subject	Acq.1	Acq. 2	Acq. 3	Acq. 4	Acq. 5
Subject 1	5.3 - 11.42	7.4 - 14.01	2,7 - 14.25	4.8 - 12	10,39 - 19,89

Table 6.2: Maximum and minimum of diameter

The percentage difference between the diameter of the first acquisition and the diameter of the others was also assessed. The variation of the maximum, minimum and subtraction between the latter was considered.

Type	Acq. 1	Acq. 2	Acq. 3	Acq. 4	Acq. 5
Max - Min	0%	+ 8%	+ 88%	+ 17%	+ 9.5%
Max	0%	+ 22%	+ 24%	+ 5%	+ 74%
Min	0%	+ 39%	- 50%	- 10%	+ 96%

Table 6.3: Percentage variation of diameters

Moreover, it has been evaluated that the coefficient of correlation found in this acquisition, has to underline and understand which, among these measures, is more accurate and reliable. However, it is important to emphasise the fact that we do not have very high correlation coefficients in all cases considered. A good coefficient can be seen in the case of the tap with increased amplitude. On the other hand, it drops dramatically in the case of raised legs, which suggests a less-than-accurate measurement and correlation. This makes third rather than fourth or fifth be preferred as a measure.

Subj.	Coeff. 1	Coeff. 2	Coeff. 3	Coeff. 4	Coeff. 5
Subject 1	0.75	0,37	0,87	0,55	0,22

Table 6.4: Maximum and minimum of diameter

## 7. Conclusion

Thus, this thesis set out to develop a low-cost spirometer that could help healthcare professionals assess RAP in emergency patients. This is also helped by the fact that not too much effort is required, but little more than is normally required for normal breathing. The on-screen display helps the treating doctor to assess the patient's actual breathing and also it helps the patient to try to overcome the boundaries.

In the future, one might think of implementing, in addition to spirometry, a device for measuring heartbeat in order to better set the frequency of cardiac beating used for the filters used for caval index evaluation.

In the end, it would be necessary to repeat these evaluations on a much larger number of patients to have a more solid statistical basis, with better and more accurate instrumentation. In addition, the performance of ultrasound scans by properly trained personnel would lead to sharper videos, which would thus make semi-automatic segmentation possible, greatly decreasing post-processing times.

In any case, the results presented in this thesis are promising since they show increases in the indicators as predicted by theory. Additionally, the option of using a semi-automatic vein tracking system offers the chance to reduce operator error and aid in more accurate calculations with rapid calculation times.



# Bibliography

- [1] Qing Zhang et al. “Relationship between inferior vena cava diameter ratio and central venous pressure”. In: *JOURNAL OF CLINICAL ULTRASOUND* 46.7 (Sept. 2018), pp. 450–454.
- [2] D.J. Lehar et al. “Inferior vena cava displacement during respirophasic ultrasound imaging”. In: *Crit Ultrasound J* 4.1 (Aug. 2012), p. 18.
- [3] Stanfield C. *Fisiologia*. Edises, 2012.
- [4] H. Gray. *Gray, Æs Anatomy: With original illustrations*. Vol. 36. Mar. 2020, pp. 1213–1225.
- [5] Sinagra G. Mesin L. Albani S. “Non-invasive Estimation of Right Atrial Pressure Using Inferior Vena Cava Echography”. In: *Ultrasound in Medicine and Biology* 45.5 (May 2019), pp. 1331–1337.
- [6] Varrias D. et al. “The Use of Point-of-Care Ultrasound (POCUS) in the Diagnosis of Deep Vein Thrombosis”. In: *J Clin Med* 17 (Sept. 2021), p. 3903.
- [7] Liou T. G. and Kanner R.E. “Spirometry”. In: *Clinical reviews in allergy immunology* 17.3 (Apr. 2017), 137, Æ152.
- [8] S. Albani et al. “Accuracy of right atrial pressure estimation using a multi parameter approach derived from inferior vena cava semi automated edge tracking echocardiography: a pilot study in patients with cardiovascular disorders”. In: *INT J CARDIOVAS IMAG* 36 (Mar. 2020), pp. 1213–1225.

- [9] International Standard. “Measurement of fluid flow by means of pressure differential devices inserted in circular cross-section conduits running full- ISO/FDIS 5167-4”. In: 4 (Dec. 2002), pp. 1–32.
- [10] Ermini L.and Seddone S. et al. “The Cardiac Caval Index: Improving Noninvasive Assessment of Cardiac Preload”. In: *Journal of Ultrasound in Medicine* 41.9 (Dicember 2021), pp. 2247–2258.
- [11] Ciozda W., Khandwalla R. Kedan I.and Kehl D.W.and Zimmer R., and Kimchi A. “The efficacy of sonographic measurement of inferior vena cava diameter as an estimate of central venous pressure”. In: *Cardiovascula ultrasound* 14 (Aug. 2016).

# List of Figures

2.1	Heart valves . . . . .	10
2.2	ECG . . . . .	11
2.3	Differences between arteries and veins . . . . .	13
2.4	Snell law . . . . .	17
2.5	Ultrasound's resolution . . . . .	19
2.6	Flowchart of ultrasound . . . . .	20
2.7	Ultrasound's probes . . . . .	21
2.9	Relation between volume and pressure . . . . .	25
2.10	Lungs volume and capacities . . . . .	26
3.1	Convex probe . . . . .	31
3.2	Spirometer dimentioning . . . . .	32
3.3	Tap dimentioning . . . . .	33
3.4	Flux without net . . . . .	34
3.5	Flux with net . . . . .	34
3.6	Output of sensor and conversion to flux . . . . .	36
3.7	Relation between pressure and area ratio . . . . .	37
3.8	Spirometer . . . . .	37
3.9	Domain of CFD . . . . .	38
3.10	Mesh . . . . .	39
3.11	CFD residuals . . . . .	40
3.12	Pressure . . . . .	40
3.13	Magnitude of speed . . . . .	41
3.14	Pressure and speed . . . . .	41
3.15	Vorticity . . . . .	42

3.16	Pressure CFD . . . . .	43
3.17	Velocity . . . . .	44
3.18	CFD vorticity . . . . .	45
3.19	Comparison between spirometers . . . . .	46
3.20	Signal obtained . . . . .	47
3.21	Error histogram . . . . .	48
4.1	Vein . . . . .	49
4.2	Vein . . . . .	50
4.3	Difference between mean diameters and hydraulic diameters . . . . .	50
4.4	Acquisition with increased bands . . . . .	52
5.1	Relation between flux and diameters . . . . .	53
5.2	Correlation of PSD . . . . .	54
5.3	PSD of the diameters . . . . .	55
5.4	Filtered diameters . . . . .	55
5.5	Correlation function for delay . . . . .	56
5.6	Correlation function for delay . . . . .	57
5.7	Relation between flow and diameters with tap . . . . .	58
5.8	PSD in the measure with tap . . . . .	59
5.9	PSD with diameter with tap . . . . .	60
5.10	Variation of diameters with filters . . . . .	60
5.11	Correlation function for delay with tap . . . . .	61
5.12	Allined signals with tap . . . . .	61
5.13	Diameters with augmented amplitude . . . . .	62
5.14	PSD in the measure with tap and augmented amplitude . . . . .	63
5.15	PSD of diameters with augmented amplitude . . . . .	63
5.16	Diameters with augmented amplitude . . . . .	64
5.17	Delay for the measure with augmented amplitude . . . . .	64
5.18	Allined diameter for the measure with augmented amplitude . . . . .	65

5.19	Variation of diameters with spirometry . . . . .	66
5.20	PSD of spirometry and diameters variation with raised legs . . .	66
5.21	PSD diameters variation with raised legs . . . . .	67
5.22	Variation of filtered diameters . . . . .	67
5.23	Delay between diameters variation and spirometry . . . . .	68
5.24	Allined diameters with raised legs . . . . .	68
5.25	Variation of diameters with spirometry and augmented amplitude	69
5.26	PSD of diameter variation and spirometry with leg raised and augmented amplitude . . . . .	70
5.27	PSD of diameter variation with leg raised and augmented am- plitude . . . . .	70
5.28	Variation of diameters filtered . . . . .	71
5.29	Delay of diameters variation and spirometry . . . . .	71
5.30	Allined diameters with raised legs and augmented amplitude . .	72

# List of Tables

2.1	Acoustical impedance and speed propagation . . . . .	15
3.1	Correlation . . . . .	48
5.1	Caval index first acquisition . . . . .	58
5.2	Caval index second acquisition . . . . .	62
5.3	Caval index third acquisition . . . . .	65
5.4	Caval index fourth acquisition . . . . .	69
5.5	Caval index fifth acquisition . . . . .	72
6.1	Caval index of the acquisitions . . . . .	74
6.2	Maximum and minimum of diameter . . . . .	75
6.3	Percentage variation of diameters . . . . .	76
6.4	Maximum and minimum of diameter . . . . .	76